KWR 2026.023 | Februari 2026

Development of a water quality sensor

Electrochemical Impedance Spectroscopy to monitor a broad range of (micro)contaminants in a single device

KWR

Bridging Science to Practice

Collaborating Partners

Colophon

Development of a water quality sensor
Electrochemical Impedance Spectroscopy to monitor a broad range of (micro)contaminants in a single device

KWR 2026.023 | Februari 2026

Project number
403687

Project manager
Ir. Astrid Reus

Collaborating Partners
Hypersoniq, Vopak, TWTG

Author(s)
Dr. Patrick S. Bäuerlein, Roan Streefland BSc., dr. Xin Tian, dr. Joep van den Broeke, Nienke Meekel, MSc., Gijs Vermeij, MSc. (Hypersoniq), dr. Peyman Taheri (TU Delft), Amir Mohseni Armaki, MSc. (TU Delft),

Quality Assurance
Dr. Thomas ter Laak, dr. Peter van Thienen

Sent to
Collaborating partners

This activity was co-financed with PPP funding from the Top Consortia for Knowledge and Innovation (TKIs) of the Dutch Ministry of Economic Affairs and Climate and the results are made public.

Keywords

Electrochemical impedance spectroscopy, sensor
Year of publishing
2026

More information
Dr. Patrick S. Bäuerlein
T +31 (0)30 60 69 702
E patrick.bauerlein@kwrwater.nl

PO Box 1072
3430 BB Nieuwegein
The Netherlands

T +31 (0)30 60 69 511
E info@kwrwater.nl
I www.kwrwater.nl

Summary

Large quantities of water are used worldwide for various industrial purposes and communal uses. Wastewater from e.g. petroleum or food industry, must be treated to remove a variety of chemical contaminants before it can be discharged to surface waters. It is necessary to monitor the effectiveness of this water treatment, both for operational control and to comply with regulations. However, with current monitoring methods that rely on grab sampling composite sampling or the application of sensors, timely, cost-effective detection of incidents that overload the wastewater treatment plant is not always possible. Thereby risking that such incidents will not be detected timely to take mitigating measures. While sensors enable continuous and near real time monitoring, they almost all provide information on sum-parameters. This means that the presence and/or concentration of a group of contaminants can be measured, but that no information about individual contaminants can be obtained. Currently, no sensor exists that combines the specificity and sensitivity in order to detect and identify a wide range, let alone all, possible contaminants. However, electrochemical Impedance Spectroscopy (EIS) has the promise to provide such a capacity. Therefore, the application of EIS for monitoring of water quality has been investigated.

Electrochemical Impedance Spectroscopy (EIS) is a non-destructive technique used to investigate the dynamic behaviour of electrochemical systems by measuring their response to small, frequency-dependent perturbations. It measures the dielectric properties of a sample to create a “fingerprint” of the water composition. This fingerprint contains information about the chemical components of the sample. The aim of this project is to demonstrate that the EIS technique can be used for real-time or near-real-time measurement of contaminants such as dissolved heavy metals and organic micropollutants and suspended particles, determining their concentrations and identities, in complex samples such as wastewater. Additionally, it is investigated if the EIS technique can also be used to determine the size of organic and inorganic particles in suspension.

Various contaminants were tested in this project. This report focuses mostly on inorganic contaminants because initial experiments revealed that the detection of organic contaminants will not be successfully tackled within the time-frame of this project. For that reason, various solution with single inorganic salts as well as mixtures of inorganic were analysed using the developed EIS sensors. In combination with machine learning the sensor was able to successfully identify the inorganic ions in solution as well as concentration within defined concentration windows.

After these successful bench scale experiments the sensor was installed in a inline sampler, that was connected to a pilot drinking water distribution system. One large scale system (several cubic meters of water) and a small-scale system (several litres). The goal of these experiments was to determine if the sensor can operate under the conditions typical for these systems (flow, pressure up to 2.5 bar) and is able to measure several hours without supervision. The results show that the sensor is able to perform well under the tested conditions.

In addition to these experiments, we also investigated whether the sensor is able to determine the size of particles in a suspension. A review of the literature showed that comparable sensors are capable of doing so. However, in our experiments, we could not confirm that our system can measure particle size. Even slight changes in the solution, such as temperature or CO_2 concentration, caused noticeable variations in the signal hampering size determination. If particle size can indeed be determined using EIS, its influence on the signal appears to be too weak than that of temperature or CO_2 concentration.

Contents

1 Introduction

1.1 Need for fast and reliable water monitoring

Clean water is an important resource which is threatened by the growing pressures on water sources. Accounting for 22% of freshwater withdrawals globally, industry, as a whole, is the second largest user of freshwater resources after agriculture. Industries use water in many different ways: as a raw material (e.g. in food industry or pharmaceutical manufacturing), as a solvent, for heating (including steam) or cooling and for transportation. Most of the water used in industry is not consumed and is potentially available for reuse. However, the water quality is usually degraded by the processes it has been involved in, which means it requires treatment before its reused within the industry, used for other (industrial) purposes or emitted to the environment.

Many different contaminations enter water applied in industrial processes. Although the nature of the contaminants depends on the specific industry, common pollutants include heavy metals, synthetic organic chemicals (e.g. plastics, pharmaceuticals and pesticides), natural organic substances (e.g. sugar, starch and lignin), acids and bases, nutrients (nitrogen, phosphorus), salts and pathogens. Industrial wastewater treatment aims to remove these contaminants and make the water fit for discharge (according to the discharge permits) or re-use. However, this treatment is not always fully effective, as illustrated by the continued occurrence of contamination incidents, both from regular discharges as well as accidental spills.

Recent examples of accidental spills include the pyrazole discharge in the river Meuse in the Netherlands (2015) and the trifluoroacetic acid release event in the river Neckar in Germany (2018). Examples of systematic discharges that contained unwanted pollutants include that PFAS in the river Scheldt in Belgium (2021). Furthermore, pollutants can also enter the water via other routes. Examples include leakage (4-methylcyclohexanemethanol in the Elk River chemical spill, USA, 2014), firefighting activities (mixture of synthetic organic chemicals, Sandoz chemical spill into the Rhine, Switzerland, 1986), or release from storage reservoirs or tailing ponds (cyanide and heavy metals, Baia Mare, Romania, 2000).

Although there are increasingly strict regulations in Europe that regulate water quality as well as better safety measures to prevent incidents, there is a continuing occurrence of incidents and water quality targets are not being met. For example, most Member States of the European Union are struggling to meet the targets for water quality of the Water Framework Directive (2000/60/EC). It shows that conventional legal frameworks with top-down central steering mechanisms struggle to achieve the desired water quality objectives. This is the consequence that the actions are not only driven by ecological and human health aspects but also legal and social-economic aspects.

Currently the water quality of industrial wastewater influents and effluents is monitored primarily by taking samples and analysing these either in a laboratory or directly on site. The *ex-situ* analysis has the disadvantage of a time lag between sampling and reporting but generally enables the application of more sensitive equipment that results in more detailed information received, e.g. a high-resolution mass spectrometry analysis of the water sample can be performed. Contrastingly, the *in situ* enables near real time analysis but often results in less detailed information, as the most advanced analytical tools are generally not employed at the site due to costs or impracticability. Detailed real-time monitoring of chemical changes in solutions, therefore, remains a pressing challenge to addressing the adequate monitoring of water quality (Schwarzenbach et al., 2006), enabling process control and preventing incidents if industrial wastewater treatment.

Sensors can offer a real-time in-line solution. They are usually easy to operate, and the data is received almost instantly. Some common examples of water quality sensors include temperature, pH, conductivity, UV/Vis or turbidity sensors (for details see Supplementary information - Sensor types). Although these sensors provide (near) real-time information about water quality at a more affordable price point than associated with state-of-the-art analytical chemical devices, they have their disadvantages. The foremost disadvantage is the fact that almost all the available sensors provide information only on sum-parameters. This means that the presence and/or concentration of a group of substances can be measured, but that no information about individual contaminants can be obtained, while water quality issues are often linked to individual or specific sub classes of chemicals such as heavy metals among other much less toxic cations such as sodium or calcium. A few exceptions exist, most notably ion selective sensors (ISEs), UV/Vis spectroscopy (which can measure a small number of substances specifically) and wet chemical analysers (which are essentially automated laboratory measurements quantifying one specific analyte). However, no sensor exists that has the potential to detect a wide range, let alone all, possible contaminants in combination with the capability to identify and quantify individual substances such as various mass spectrometric techniques can do. Electrochemical Impedance Spectroscopy (EIS) has the promise to provide such a capacity. Therefore, the application of EIS for monitoring of water quality in industrial effluents has been investigated.

1.2 General introduction to Electrochemical Impedance Spectroscopy

Electrochemical Impedance Spectroscopy (EIS) is a non-destructive technique used to investigate the dynamic behaviour of electrochemical systems by measuring their response to small, frequency-dependent perturbations. This method provides detailed insights into processes occurring at or near electrode interfaces, including charge-transfer reactions, double-layer formation, adsorption/desorption, and mass transport phenomena such as diffusion. Importantly, EIS enables the separation and analysis of these overlapping processes based on their characteristic frequency responses. In EIS the impedance is measured at a series of frequencies, each providing a sinusoidal response of measured current following applied potential (Figure 1).

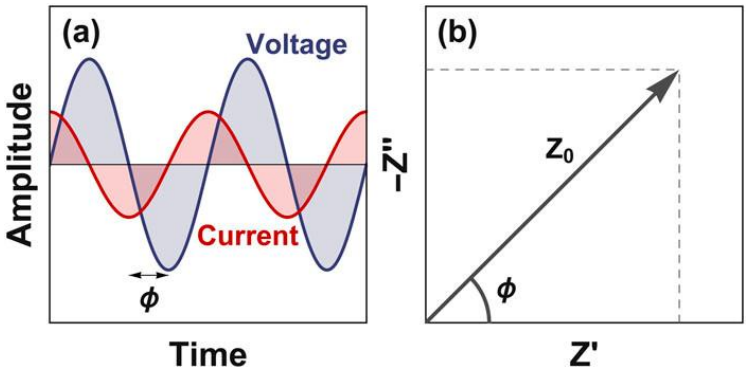

Figure 1: Example of a) an impedance measurement response plot, with both applied voltage and measured current at one frequency being shown and b) phase angle Φ and impedance expressed as the modulus Z_0 (Futscher et al., 2020).

At its core, this involves applying a low-amplitude sinusoidal voltage or current signal to a system and measuring the resulting current or voltage response. Depending on the input type, the approach is categorized as potentiostatic (voltage input) or galvanostatic (current input). This perturbation is typically swept across a wide frequency range—often from megahertz (MHz) down to millihertz (mHz)—allowing the system's response to be analysed across a broad spectrum of dynamic behaviour.

Impedance, denoted as **Z**, generalizes resistance in alternating current (AC) systems and is typically expressed as a complex quantity comprising a magnitude and a phase angle (Φ). Unlike resistance in direct current (DC) systems—described by Ohm's Law ($E = I \cdot R$)—impedance in AC systems follows the relationship $E = I \cdot Z$. The wave nature of the signals necessitates two parameters: the **impedance modulus** and the **phase shift**. These parameters reflect the system's opposition to charge movement, incorporating contributions from resistive, capacitive, and inductive elements.

In practice, a standard EIS setup consists of a working, reference, and counter electrode. A known voltage is passed from the working electrode through an electrolytic solution into the counter electrode, resulting in sample polarization. The response current has the same frequency but typically differs in phase and amplitude. From this, the impedance at each frequency is calculated.

Impedance data are most commonly visualized through **Nyquist plots** and **Bode plots** (Figure 2). In a Nyquist plot the real component of impedance is plotted on the x-axis and the negative imaginary component on the y-axis. In contrast, a Bode plot (Figure 2b) shows the magnitude and phase of the impedance as a function of frequency. While both plots contain equivalent information, the Nyquist plot is often preferred for distinguishing between dielectric processes, whereas Bode plots can offer clearer insights into frequency-dependent behaviour.

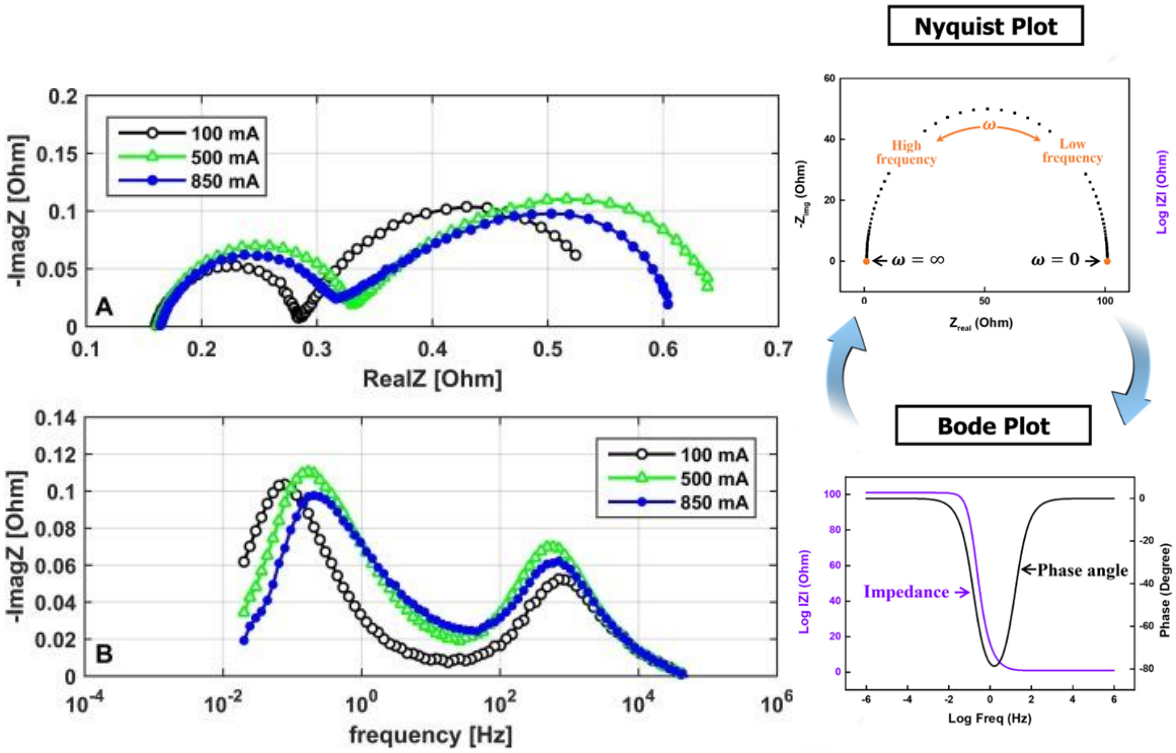

Figure 2: Examples of an experimental Nyquist (top left) and Bode (bottom right) plot (Zago and Casalegno, 2017). Examples of illustrative Nyquist (top right)t and Bode (bottom right) plots (Choi et al., 2020)

Dielectric Mechanisms and Frequency Dependence

The ability of a system to store and transfer charge is influenced by various **dielectric mechanisms**, which determine how a material polarises in response to an electric field. Each mechanism is associated with a **characteristic frequency**, which corresponds to the inverse of the characteristic time of the process. These mechanisms generally fall into two categories: **relaxation** and **resonance**.

From high to low frequency, the primary dielectric mechanisms include:

- **Electronic polarization**: Involves displacement of the electron cloud relative to the nucleus in neutral atoms.
- **Atomic polarization**: Occurs when bonded positive and negative ions stretch under an electric field.
- **Dipole polarization**: Arises from permanent or induced molecular dipoles aligning with the external field. Dipole relaxation depends heavily on temperature and the local chemical environment due to its sensitivity to viscosity and molecular interactions.
- **Ionic polarization**: Results from ionic conductivity and interfacial relaxation processes, particularly dominant at low frequencies due to charge separation across greater distances.
- **Dielectric relaxation**: Encompasses the combined effects of dipole and ionic relaxation, typically observed in the frequency range of 10^2–10^{10} Hz, which aligns with the operating window of EIS.

Each mechanism contributes to the overall impedance response, as illustrated in Figure 3, showing how different components of permittivity (real and imaginary) vary with frequency.

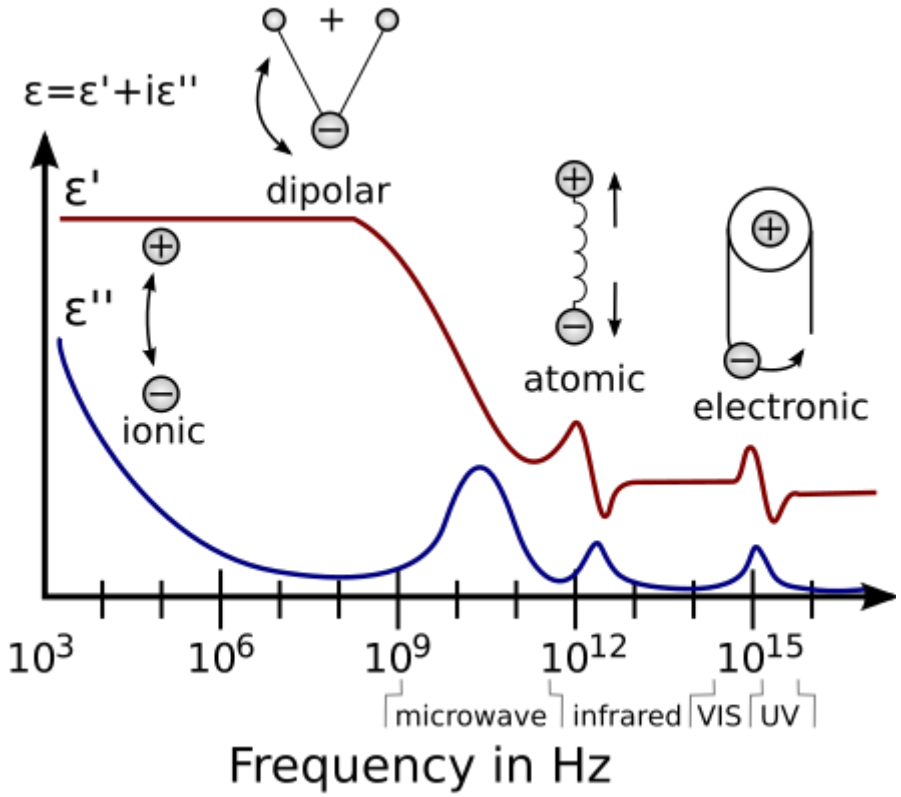

Figure 3: An illustration of the frequency response of various dielectric mechanisms in terms of the real and imaginary parts of the permittivity. The processes analysed using EIS are in the 10^2-10^{10} Hz. Image used with the consent of Prof. Kenneth A. Mauritz. (Mauritz)

Interpretation of EIS Data

A central challenge in EIS lies in interpreting the complex impedance spectra, especially when analysing mixtures or real-world samples like water. In simple systems, **Equivalent Electrical Circuit (EEC)** models are employed, representing the system as combinations of ideal circuit elements (resistors, capacitors, and inductors), each corresponding to a physical process—e.g., double-layer capacitance or charge transfer resistance.
However, this modelling approach becomes increasingly ambiguous in complex systems where numerous overlapping mechanisms and components influence the response. For instance, the EIS spectrum of a pure ionic species in water reflects the dielectric behaviour of that single compound. But in mixtures, the spectrum is essentially a "fingerprint" of all species present, making it difficult to disentangle contributions from individual analytes. The complexity is compounded by the simultaneous action of multiple dielectric mechanisms across

different time scales. Nonetheless, EIS remains a uniquely powerful tool because it allows processes to be separated by frequency rather than time, as in many DC techniques. Fast processes such as double-layer charging dominate the high-frequency region, while slower phenomena like diffusion manifest at low frequencies. This temporal resolution allows for more precise characterization of the composition of a solution and system diagnostics.

A comprehensive introduction to EIS has been written by Lazanas *et. al.* (Lazanas and Prodromidis, 2023).

1.3 Potential benefits of EIS for water quality analysis

As described above, EIS is a theoretically complex method. It is challenging to distinguish the different dielectric mechanisms and their effects, which becomes even more complicated when mixtures in complex matrices are measured. As a result, the wide scale application of EIS has remained limited to a small number of fields such as the characterisation of electronic systems (especially batteries and Li batteries in particular), characterization of coatings, and in corrosion analysis. The big advantage of EIS for the application as a water quality sensor is that it is a non-destructive measurement (it does not alter the matrix being measured).

The EIS technology seems promising for the analysis of liquid samples. Detection of metal ions as well as organic compounds have been reported, e.g. phthalates and triclosan are detectable in water using EIS sensors, and EIS can be used to detect anionic surfactants in water-oil emulsions. At the moment, however, its use on liquid samples remains limited to research applications. This is primarily due to the complexity of the signals and the need for very accurate and precise systems. With the increasing computational power available (including modelling and AI), more advanced EIS applications are now becoming possible.

What added value can a sensor based on EIS offer to the already extensive spectrum of water quality sensors?
First and foremost, the generic nature of the measurement principle means that theoretically EIS can be used to detect any type of substance. Due to the various dielectric processes it triggers, it can measure both ionic and neutral substances. This is a unique feature, as all currently available technologies, except for refractive index measurements, are sensitive to a specific subset of compounds. Furthermore, each substance has a specific impedance response at different frequencies. By scanning through multiple frequencies, an impedance spectrum can be obtained that is characteristic for the specific substance. This offers the potential for a sensor that can classify, or potentially identify, compounds present in a sample/flow and its concentration.

EIS shares the operational benefits with other electrochemical methods that the measurement is non-destructive (sample is not altered), fast (seconds-minutes measurement frequency), and does not require chemicals or sample preparation. The fact that it is a fully solid-state technique, with the sensing element made from corrosion resistant materials (e.g. platinum, gold), forms the basis for a robust and durable sensor.

In summary, Electrochemical Impedance Spectroscopy (EIS) offers several significant advantages that make it a valuable tool for chemical detection and analysis. It is highly sensitive and capable of detecting a wide variety of chemical substances simultaneously using a single sensor, including those for which no commercial sensors currently exist—such as saturated hydrocarbons, sugars, and certain solvents. EIS also has the potential to classify both groups of chemicals and individual compounds based on their unique impedance spectra. By providing a characteristic “fingerprint” of a water sample, it enables the detection of changes in matrix composition, offering early warning of deviations or incidents. The technique is fast, requires no additional chemicals or reagents, and is non-destructive, preserving the sample for further testing or analysis.

1.4 Potential drawbacks of EIS for water quality analysis

The analysis of micropollutants in water using EIS is a relatively new application. As it is not developed to its full potential yet, real drawbacks on the sensor performance are difficult to predict. However, it is expected that the major challenges will involve the sensor robustness and the data analysis. Deposition of sample residues might affect the measurement performance of the sensor and therefore the results. Moreover, the technique is very sensitive to the surrounding environment and can (at the time of writing) only be operated inside a Faraday cage and therefore requires a quite bulky setup. For applications in an industrial environment, which can have strong and fluctuating electric and magnetic fields, e.g. from turbine engines, insulation of the sensor from this environment would be required. Another potential drawback of the EIS technology is the sensitivity for analytes alongside the background signals – at present sensitivity in the low mg/L concentration range is reported. This might be sufficient for some applications, but especially in effluent and surface water monitoring, µg/L concentrations need to be detectable even against a strong and changeable background matrix. The ability of EIS to differentiate between the target analytes and the matrix, i.e. its ability to detect and identify specific compounds in a complex matrix, remains unproven and was investigated here in the TKI Watertechnologie project “Ontwikkeling van een waterkwaliteit sensor met behulp van Elektrochemische Impedantie Spectroscopie voor het meten van (micro)verontreinigingen”.

2 Measurement of salt solutions

2.1 Platinum chips

Experimental EIS data were collected using a two-electrode system. Platinum inter-digitated electrodes were designed and fabricated on a silicon chip (Figure 4) with a silicon nitride isolation layer. The electrodes were deposited using a physical vapor deposition (PVD) method, achieving a flat surface with a roughness of approximately 5 nm. The inter-digitated configuration increased the effective surface area, and the electrode spacing was set at 10 µm to minimize bulk impedance effects.

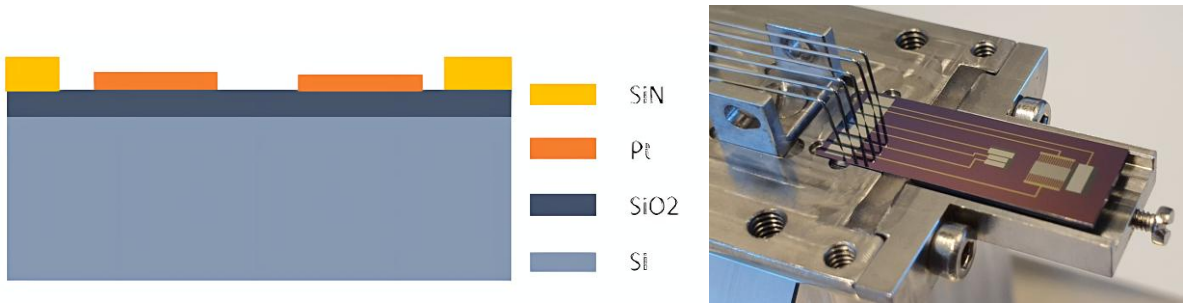

Figure 4: Sketch of the different parts of the chips (left). Picture of the platinum chip (right).

2.2 Impedance measurements

Rinse a 25 mL polypropylene-beaker with the solution to be measured and fill it to approximately 20 mL. Place the beaker in the water-jacketed cell on a 3D-printed beaker mount as shown in (Figure 5, left). The sensor is then placed on top of the water-jacketed cell (Figure 5 middle). The chip should be completely immersed in the solution. If the chip is not fully immersed change the height of the beaker mount. Move the sensor up and down once to get rid of any air bubbles on the chip surface. Figure 5 (right) shows how to connect the BioLogic potentiostat to the sensor. Connect the plugs of the red P1 with S1 and then connect the wire to the top red socket of the sensor (Working electrode, WE). Connect the blue P2 to S3 and insert it into the top blue socket of the sensor (counter electrode, CE). Then connect the white S2 to the top white connector of the sensor (reference electrode, REF). If a measurement is needed without the reference electrode, the white wire is inserted into the back of the P2 wire. When using the PalmSens potentiostatr, the black wire is connected to the reference electrode of the sensor (white connection). The red and blue wires are connected in the same way as for the Biologic potentiostat. The water-jacketed cell in placed in Faraday cage (Figure 6). The settings for the potentiostats can be found in **Error! Reference source not found.**. For each solution a Nyquist and a Bode plot were acquired (see examples Figure 7 and Figure 8).

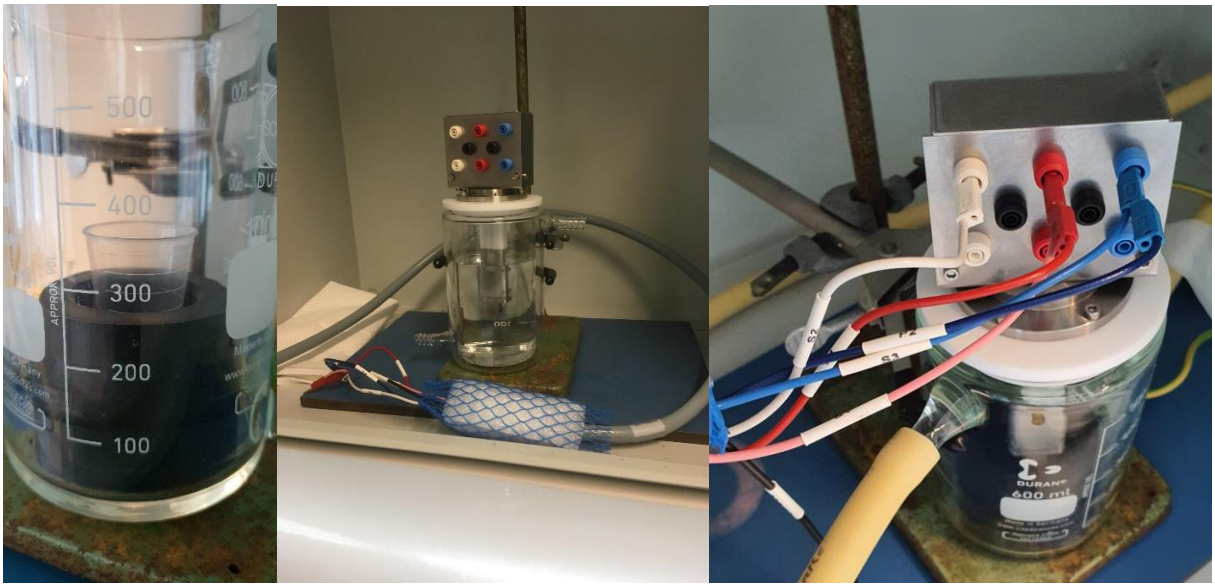

Figure 5: Setup of the measuring cell.

Figure 6: EIS-setup. BioLogic potentiostat (SP-200), Faraday cage with measuring cell and a Julabo temperature control unit.

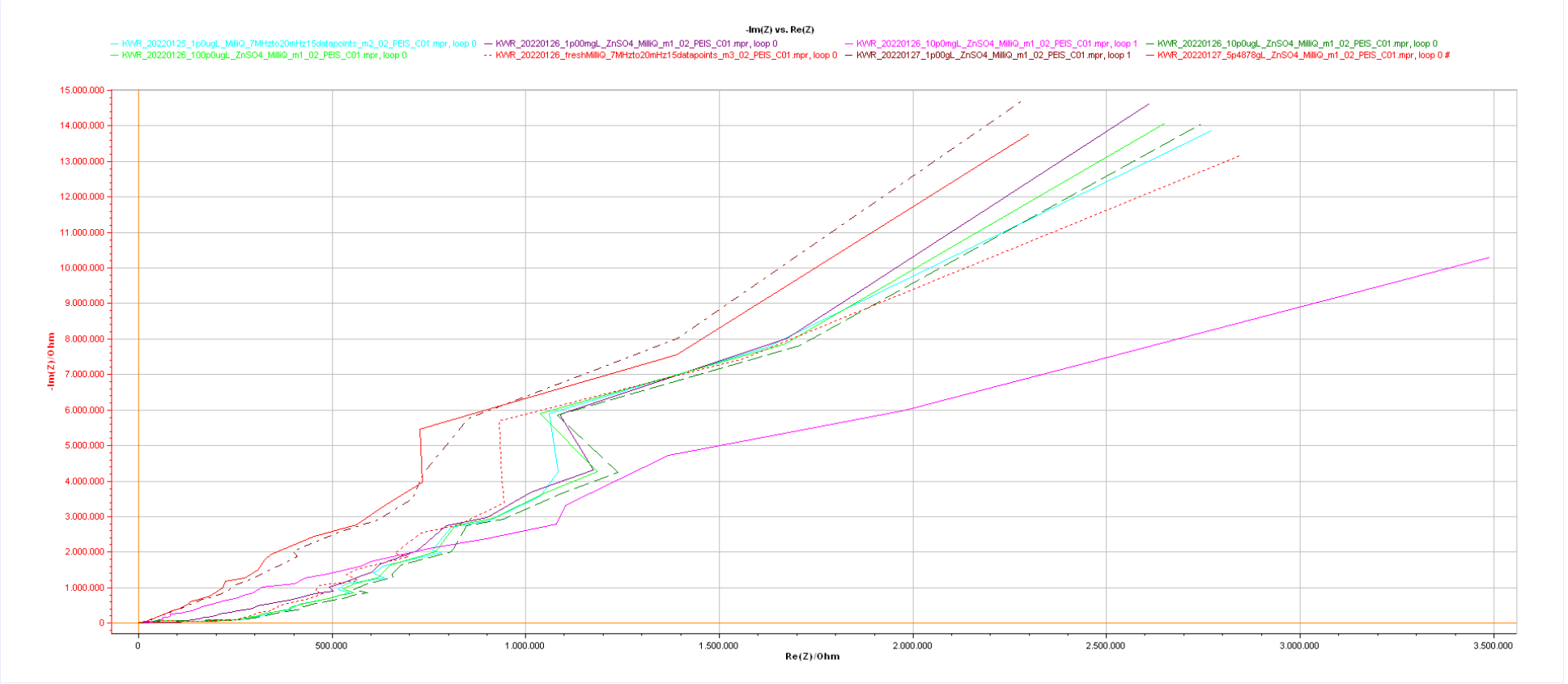

Figure 7: Bode plot, $ZnSO_4$ at different concentrations

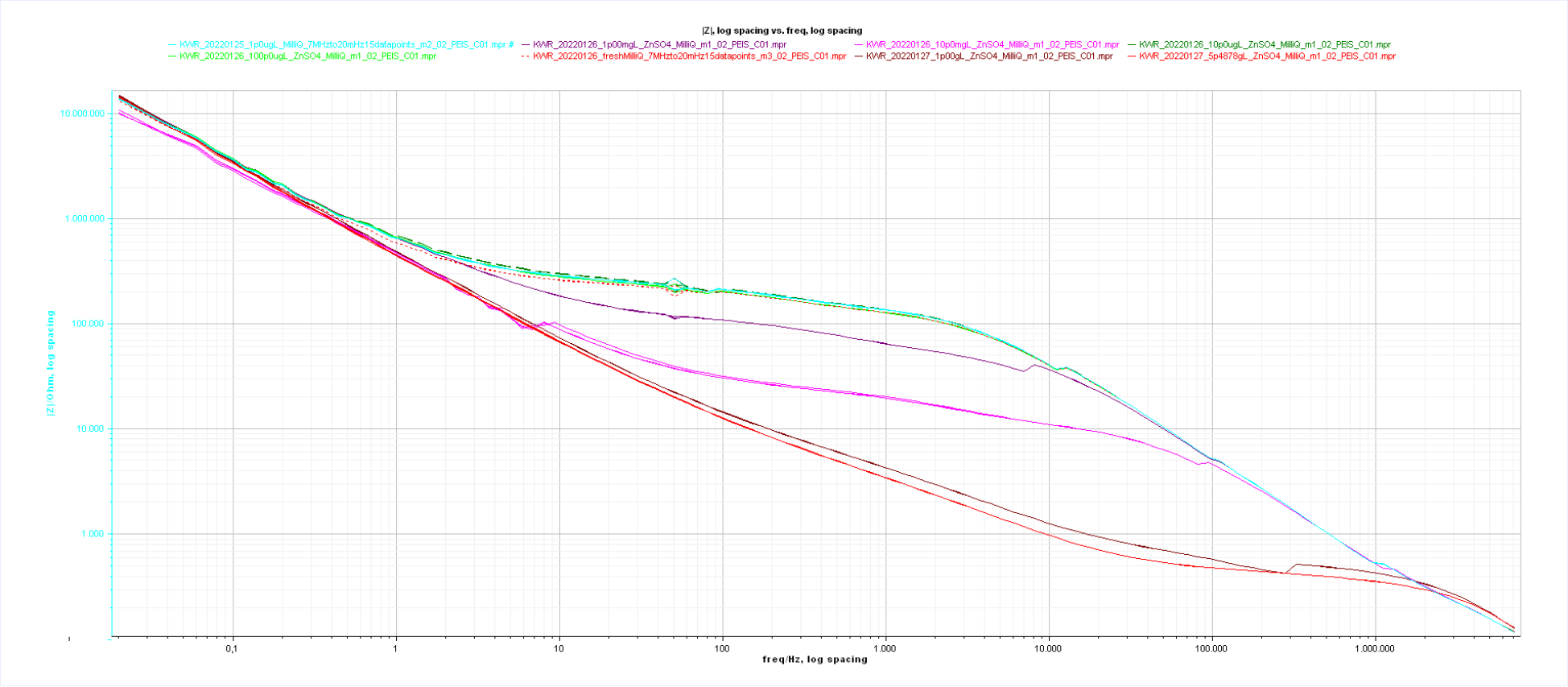

Figure 8: Bode plot, $ZnSO_4$ at different concentrations

2.3 Cleaning protocol

The first step was to ensure repeatability of the experiments. Repetitive analysis of the same solution under the same conditions lead to different results, illustrating that the analysis was not stable. For this reason, a cleaning protocol was developed, that ensured repeatability.

Chips are cleaned by following a `RCA 1`- and `RCA 2`-procedure when chips are new and when results are not as expected. The RCA procedures are described below.

RCA-1
Fill a beaker with 40 ml ultra-pure water and 8 ml NH_4OH (27 %) and heat to 70-75 °C on a hotplate. Then add 8 ml H_2O_2 (30 %). Turn off the hotplate and carefully place the chips in the solution. The solution will start to bubble after a couple of minutes. Use an ABS pincet to push any floating chips under so the chips are in complete contact with the solution. Let it stand for approximately 10 - 15 minutes. Then transfer the chips to another beaker and flush the beaker with ultra-pure water in the sink so the volume is refreshed a couple of times.
The purpose of the RCA-1 procedure is to remove organic contaminants from the chip surface.

RCA-2
Fill a beaker with 30 ml ultra-pure water and 5 ml HCl (27 %). Follow the same procedure as for RCA-1, but add 5 ml H_2O_2 (30 %) to the heated HCl solution. The purpose of the RCA-2 procedure is to remove complexed metal ions from the chip surface.

In between measurements when changing solutions the sensor is removed, and the bottom section is rinsed with ultra-pure water (18.2 MΩ·cm) and dried under a nitrogen gas stream.

2.4 Solutions and mixture measurement

For the following ions solutions were prepared:

Table 1: Table of the different ions.

Ion	Charge
Zn^{2+}	+2
Cd^{2+}	+2
Pb^{2+}	+2
Mg^{2+}	+2
Cl^-	−1
NO_3^-	−1
SO_4^{2-}	−2
Na^+	+1
K^+	+1
NH_4^+	+1
OH^-	−1
$H_2PO_4^-$	−1
HPO_4^{2-}	−2
MilliQ water	n.a.

Concentrations between 0.001 mmol/L and 20.0 mmol/L (from microgram to milligram) for each of these ions were prepared by dissolving salts in MilliQ water.

Furthermore, several binary and tertiary salt solution with various ratios were prepared.

Table 2: Table with the different solutions that were prepared.

Mixture	Ratio
$ZnNO_3$ / $Cd(NO_3)_2$	3:1
$ZnNO_3$ / $Cd(NO_3)_2$	1:1
$ZnNO_3$ / $Cd(NO_3)_2$	1:3
$PbNO_3$ / $Cd(NO_3)_2$	3:1
$PbNO_3$ / $Cd(NO_3)_2$	1:1
$PbNO_3$ / $Cd(NO_3)_2$	1:3
$ZnSO_4$ / $CdSO_4$	3:1
$ZnSO_4$ / $CdSO_4$	1:1
$ZnSO_4$ / $CdSO_4$	1:3
$Zn(NO_3)_2$ / $ZnCl_2$	3:1
$Zn(NO_3)_2$ / $ZnCl_2$	1:1
$Zn(NO_3)_2$ / $ZnCl_2$	1:3
$Zn(NO_3)_2$ / $ZnSO_4$	3:1
$Zn(NO_3)_2$ / $ZnSO_4$	1:1
$Zn(NO_3)_2$ / $ZnSO_4$	1:3
$ZnCl_2$ / $ZnSO_4$	3:1
$ZnCl_2$ / $ZnSO_4$	1:1
$ZnCl_2$ / $ZnSO_4$	1:3
$Pb(NO_3)_2$ / $Zn(NO_3)_2$ / $Cd(NO_3)_2$	1:1:2
$Pb(NO_3)_2$ / $Zn(NO_3)_2$ / $Cd(NO_3)_2$	1:2:1
$PbCl_2$ / $ZnCl_2$ / $CdCl_2$	1:1:20
$PbCl_2$ / $ZnCl_2$ / $CdCl_2$	1:2:20

3 Identification and quantification of ions in solution using AI-powered models

3.1 Reading the EIS measurements

As processing EIS measurements is a new development to KWR, the initial step was reviewing the data format. We noticed that each measurement was stored in an mpt format, which is an ASCII file that can be opened using a notebook. Particularly, the EIS data file begins with a metadata section summarizing the experimental setup and acquisition parameters, followed by the recorded measurement values. Regarding our measurements, the experiment was performed using a Bio-Logic EC-Lab system (software v11.43, firmware v1.41). This selected example electrolyte solution (see Figure 9) consisted of a $ZnSO_4$ solution, with a characteristic electrode surface area of 1.160 mm² and mass of 0.001 g. The metadata also contains other details such as instrument settings, electrode specifications, and acquisition parameters, which are followed by the tabulated experimental results.

To process the file programmatically, the entire file is first read as plain text so that both the metadata and numerical sections can be preserved. The position of the table is then located by searching for the first occurrence of the string ‘freq/Hz’. All lines before this position are regarded as metadata and stored separately. The header line with ‘freq/Hz’ and all subsequent rows form the measurement dataset.

KWR_20230109_ZnSO4_100nmolL_MQ_m1_ID5A_NoRef_BW8_02_PEIS_C01.mpt - Notepad

File Edit Format View Help

```
EC-Lab ASCII FILE
Nb header lines : 70

Potentio Electrochemical Impedance Spectroscopy

Run on channel : 1 (SN 13470)
User : Roan
Electrode connection : standard
Potential control : Ewe
Ewe ctrl range : min = -10.00 V, max = 10.00 V
Ewe,I filtering : 50 kHz
Safety Limits :
        Do not start on E overload
Channel : Floating
Acquisition started on : 01/09/2023 16:24:37.452
Technique started on : 01/09/2023 16:34:41.322
Loaded Setting File :  NONE
Saved on :
        File : KWR_20230109_ZnSO4_100nmolL_MQ_m1_ID5A_NoRef_BW8_02_PEIS_C01.mpr
        Directory : D:\Users\lmcdata\Documents\EC-Lab\Data\20230109\
        Host : 10.1.20.99
Device : SP-200 (SN 1139)
Address : USB
EC-Lab for windows v11.43 (software)
Internet server v11.40 (firmware)
Command interpretor v11.43 (firmware)
Electrode material : Platinum
Initial state :
Electrolyte :
Comments : Ref Electrode set to unspecified, ID-5
Cable : standard
Electrode surface area : 1.160 mm²
Characteristic mass : 0.001 g
Equivalent Weight : 0.000 g/eq.
Density : 0.000 g/cm3
Volume (V) : 0.001 cm³
Record EIS quality indicators
Text export
   Mode : Standard
   Time format : Elapsed
Cycle Definition : Charge/Discharge alternance
Mode                Single sine
E (V)               0.0000
vs.                 Eoc
tE (h:m:s)          0:00:0.0000
record              0
dI                  0.000
unit dI             mA
dt (s)              0.005
fi                  7.000
unit fi             MHz
ff                  20.000
unit ff             mHz
Nd                  20
Points              per decade
spacing             Logarithmic
Va (mV)             10.0
pw                  0.10
Na                  1
corr                1
E range min (V)     -10.000
E range max (V)     10.000
I Range             Auto
Bandwidth           8
nc cycles           2
goto Ns'            0
nr cycles           0
inc. cycle          1

freq/Hz Re(Z)/Ohm       -Im(Z)/Ohm      |Z|/Ohm Phase(Z)/deg    time/s  <Ewe>/V <I>/mA  Cs/µF   Cp/µF   cycle number    I Range |Ewe|/V |I|/A   Ns      (Q-Qo)/mA.h     THD Ewe/%       NSD Ewe/%
7.0000185E+006  2.0095952E+002  3.2519025E+002  3.8227402E+002  -5.8284962E+001 6.038700302264624E+002  -3.3622760E-002 -6.5328095E-005 6.9917107E-005  5.0595154E-005  1.000000000000000E+000  40
6.2350340E+006  2.2406358E+002  3.4844928E+002  4.1427213E+002  -5.7257740E+001 6.047630355488946E+002  -3.3612635E-002 -3.0931133E-005 7.3255753E-005  5.1826206E-005  1.000000000000000E+000  40
5.5536670E+006  2.4318465E+002  3.6070187E+002  4.3502255E+002  -5.6012215E+001 6.052770469332900E+002  -3.3613585E-002 -2.7502641E-005 7.9449630E-005  5.4621691E-005  1.000000000000000E+000  40
4.9467505E+006  2.7042273E+002  3.8683829E+002  4.7198761E+002  -5.5044186E+001 6.056473498309351E+002  -3.3622891E-002 -3.1546006E-005 8.3170758E-005  5.5868677E-005  1.000000000000000E+000  40
4.4061665E+006  2.7884393E+002  4.0666656E+002  4.9308380E+002  -5.5562271E+001 6.060183500085550E+002  -3.3637624E-002 -3.0595715E-005 8.8822046E-005  6.0416594E-005  1.000000000000000E+000  40
```

Figure 9: An example file for the .mpt format (Example: KWR_20230109_ZnSO4_100nmolL_MQ_m1_ID5A_NoRef_BW8_02_PEIS_C01.mpt).

3.1.1 Brief introduction of the EIS raw data

Following the separation of metadata from the .mpt file, the retrieved measurement dataset consisted of multiple columns representing frequency-domain electrochemical parameters (Figure 10), which include:

- freq (Hz) – Applied AC signal frequency.
- ReZ (Ω) – Real component of the impedance (resistive part).
- ImZ (Ω) – Imaginary component of the impedance (reactive part).
- Z (Ω) – Magnitude of the impedance, calculated as the square root of the sum of the squares of its real component (ReZ) and imaginary component (ImZ).
- PhaseZ (°) – Phase angle between voltage and current, calculated as the arctangent of the ratio of ImZ to ReZ.
- time (s) – Elapsed time since the start of the measurement.
- Ewe (V) – Measured working electrode potential.
- I (mA) – Measured current.
- Cs (F) – Series capacitance, derived from the impedance at the given frequency.
- Cp (F) – Parallel capacitance, also derived from the impedance response.
- cycleNumber – Identifier for the measurement cycle within the experiment.

	1 freqHz	2 ReZOhm	3 ImZOhm	4 ZOhm	5 PhaseZdeg	6 times	7 EweV	8 ImA	9 CsF	10 CpF	11 cycleNumber
1	7.0000e+06	200.9595	325.1903	382.2740	-58.2850	603.8700	-0.0336	-6.5328e-05	6.9917e-05	5.0595e-05	1
2	6235034	224.0636	348.4493	414.2721	-57.2577	604.7630	-0.0336	-3.0931e-05	7.3256e-05	5.1826e-05	1
3	5553667	243.1847	360.7019	435.0226	-56.0122	605.2770	-0.0336	-2.7503e-05	7.9450e-05	5.4622e-05	1
4	4.9468e+06	270.4227	386.8383	471.9876	-55.0442	605.6473	-0.0336	-3.1546e-05	8.3171e-05	5.5869e-05	1
5	4.4062e+06	278.8439	406.6666	493.0838	-55.5623	606.0184	-0.0336	-3.0596e-05	8.8822e-05	6.0417e-05	1
6	3.9247e+06	295.4565	430.0415	521.7569	-55.5093	606.3894	-0.0336	-3.2273e-05	9.4299e-05	6.4061e-05	1
7	3495769	311.3518	455.5263	551.7645	-55.6474	606.7604	-0.0337	-3.3726e-05	9.9946e-05	6.8121e-05	1
8	3.1137e+06	325.9196	484.5288	583.9450	-56.0731	607.1314	-0.0337	-3.0582e-05	1.0549e-04	7.2629e-05	1
9	2.7735e+06	339.3492	518.1920	619.4198	-56.7804	607.5024	-0.0336	-5.2150e-05	1.1074e-04	7.7503e-05	1
10	2470383	347.9047	560.1199	659.3724	-58.1545	608.0171	-0.0336	-6.2914e-05	1.1502e-04	8.2999e-05	1
11	2200425	354.4000	606.4884	702.4440	-59.7002	608.3874	-0.0337	-3.9718e-05	1.1926e-04	8.8902e-05	1
12	1959954	360.7736	656.4542	749.0592	-61.2077	608.9020	-0.0337	-7.6289e-05	1.2370e-04	9.5005e-05	1
13	1745769	367.4421	719.3425	807.7545	-62.9419	609.4160	-0.0337	-5.2836e-05	1.2674e-04	1.0051e-04	1
14	1.5550e+06	370.4266	789.3369	871.9338	-64.8599	609.9301	-0.0337	-3.8017e-05	1.2967e-04	1.0626e-04	1
15	1.3851e+06	379.0749	868.1495	947.3022	-66.4117	610.3004	-0.0337	-5.0006e-05	1.3236e-04	1.1117e-04	1
16	1.2337e+06	381.9728	957.4864	1.0309e+03	-68.2513	610.8150	-0.0337	-2.3990e-06	1.3473e-04	1.1624e-04	1
17	1098881	384.7737	1.0636e+03	1.1310e+03	-70.1110	611.3290	-0.0337	-2.7473e-05	1.3618e-04	1.2042e-04	1
18	9.7879e+05	390.0772	1.1801e+03	1.2429e+03	-71.7083	611.8440	-0.0337	-2.4835e-05	1.3779e-04	1.2422e-04	1
19	8.7183e+05	388.4660	1.3146e+03	1.3708e+03	-73.5372	612.3591	-0.0337	-1.7906e-05	1.3887e-04	1.2772e-04	1
20	7.7656e+05	396.3434	1.4598e+03	1.5127e+03	-74.8103	612.8740	-0.0337	3.8120e-05	1.4039e-04	1.3076e-04	1
21	6.9169e+05	396.1539	1.6352e+03	1.6825e+03	-76.3814	613.5320	-0.0337	-2.5035e-05	1.4071e-04	1.3291e-04	1
22	6.1610e+05	407.5386	1.8287e+03	1.8735e+03	-77.4363	614.0470	-0.0337	-2.7856e-05	1.4126e-04	1.3458e-04	1
23	5.4878e+05	405.1410	2.0387e+03	2.0786e+03	-78.7602	614.5620	-0.0337	-5.2515e-05	1.4226e-04	1.3685e-04	1
24	4.8880e+05	415.2662	2.2763e+03	2.3139e+03	-79.6614	615.0771	-0.0337	-3.6443e-05	1.4304e-04	1.3843e-04	1
25	4.3538e+05	420.5310	2.5481e+03	2.5826e+03	-80.6286	615.5920	-0.0337	-4.3683e-05	1.4346e-04	1.3966e-04	1
26	3.8780e+05	427.3648	2.8648e+03	2.8965e+03	-81.5154	616.2500	-0.0337	-1.9774e-06	1.4325e-04	1.4014e-04	1
27	3.4543e+05	440.5333	3.1955e+03	3.2257e+03	-82.1506	616.7650	-0.0337	-7.0080e-05	1.4419e-04	1.4150e-04	1
28	3.0768e+05	445.2014	3.5992e+03	3.6266e+03	-82.9486	617.2790	-0.0337	-3.6453e-05	1.4372e-04	1.4156e-04	1
29	2.7406e+05	454.0374	4.0169e+03	4.0424e+03	-83.5511	617.7940	-0.0337	-4.1152e-05	1.4457e-04	1.4275e-04	1

Figure 10 Raw data of the EIS measurements.

Note that since columns six to eleven are less relevant, only the first five columns (freq, ReZ, ImZ, Z and phase) are considered in our following analysis. The remaining columns are only saved for reference purposes.

3.1.2 Visualization of EIS in an Euclidean (Cartesian) coordinate system

To gain an initial understanding of the electrochemical impedance behaviour, for instance on the example measurement - $ZnSO_4$ (100 nmol/L), we first visualized the real (ReZ) and imaginary (ImZ) components of impedance as functions of frequency. The frequency axis is plotted on a logarithmic scale to capture the wide frequency range (up to 10^8), while the impedance components are plotted on a linear scale. In doing so, we can observe the trends and magnitude differences between the resistive and reactive parts of the impedance across frequencies (Figure 11). In this example measurement, both the real and imaginary components of impedance, at low frequencies, show relatively high values, indicating significant resistance and reactance in the system. This implies that ion mobility effects dominate at low frequencies. As the frequency increases, the impedance decreases sharply, reaching very low values at high frequencies. This behaviour reflects the reduced influence of interfacial polarization and the improved ability of ions to follow the alternating electric field at higher frequencies.

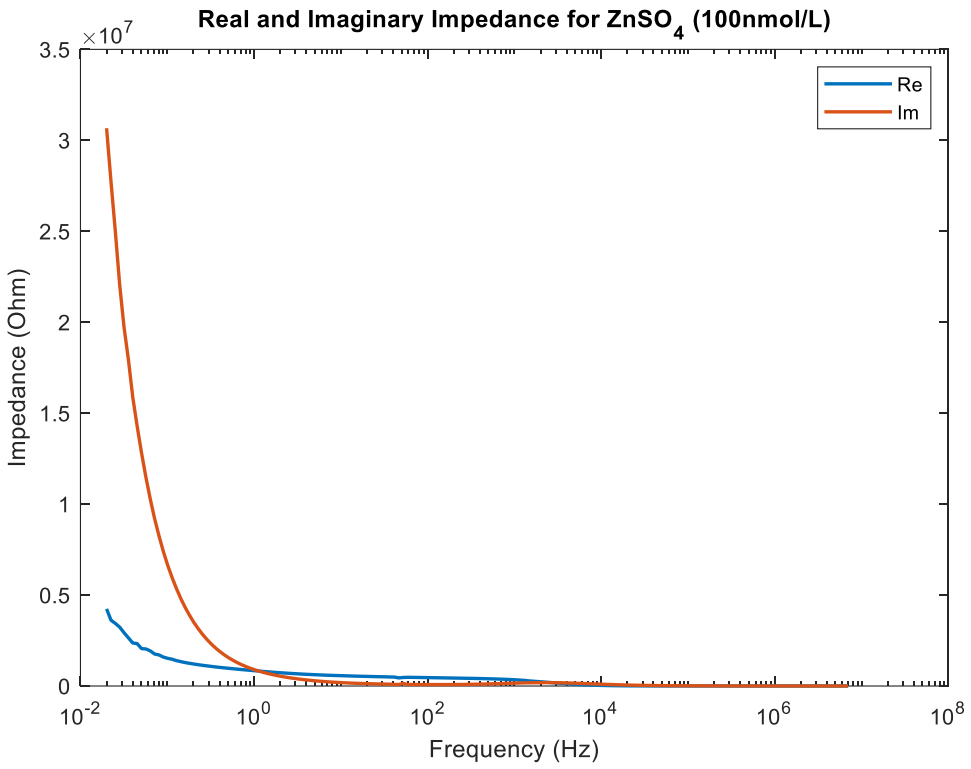

Figure 11 Real and imaginary impedance visualized in Euclidean coordinates.

3.1.3 Visual enhancement of EIS in an polar coordinate system

To enhance interpretation of the impedance data, the original signals were transformed from their Cartesian form (real and imaginary components) into a polar system. To do so, the fourth column (Z) was first transformed using the natural logarithm to compress its dynamic range and stabilize variance while the fifth column (Phase) was shifted by +360° to avoid discontinuities at the wrap-around point prior to smoothing. Next. both Z and Phase were smoothed using a moving-mean filter with a window of 30 samples to attenuate high-frequency noise while preserving overall trends. After smoothing, per-sample minima and maxima were computed for both Z and Phase. Using these minima and maxima, Phase was linearly rescaled to span the full angular domain [0,2π], while Z was linearly mapped to the unit interval [0,1], in order to ensure that all samples share the same scale for visual presentations and follow-up analyses. The resulting representation is then visualized in polar plots (Figure 12).

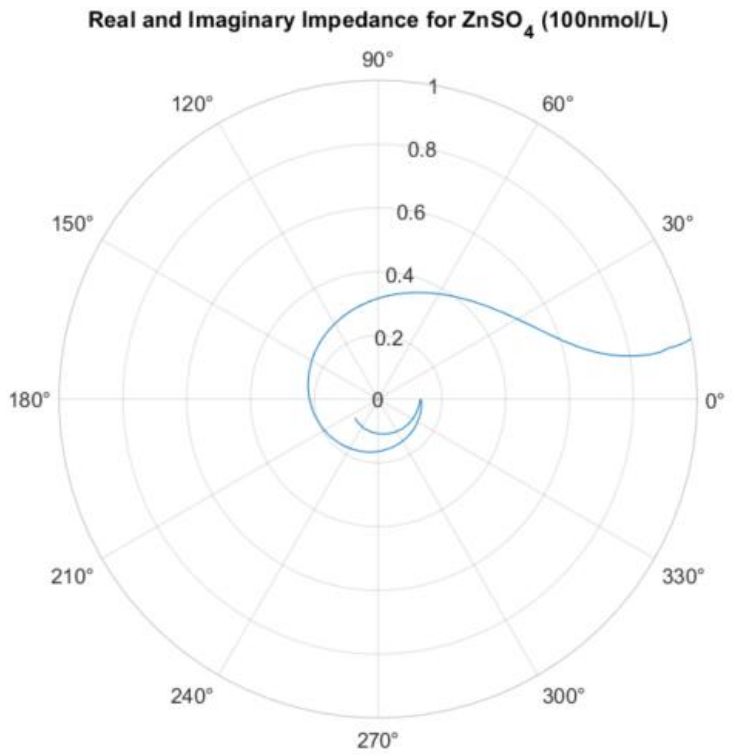

Figure 12 Impedance visualized in polar coordinates

In doing so, we are able to visualize all EIS measurements in polar coordinates. Figure 13, Figure 14, and Figure 15 show three groups of EIS measurements in different solutions – 10 mmol/l, 10 µmol/l, and 100 nmol/l. By comparison of these three groups, we can clearly see that the impedance spectra vary significantly with concentration. At higher concentrations (10 mmol/L), the curves tend to cluster closer to the inner radial region after 30 degrees while at lower concentrations (100 nmol/L), the curves shift outward. Note that there is also a strong group characteristic: solutions with the same concentration show high similarity, forming visually cohesive clusters on the polar plots. At the same time, there are clear differences between the groups, both in radial position and angular distribution. These visual presentations have three-fold purposes:

1. They provide laboratory analysts with a new, intuitive and clear way to interpret impedance spectra, making it easier to identify patterns and anomalies.
2. They provide our partner TU Delft an inspiring data pre-processing step in developing a concentration prediction model (which is excluded from this report).
3. They enable KWR to use these visuals to build a classification model based on the group characteristics observed in the polar plots to differentiate different solutions (Section 3.2).

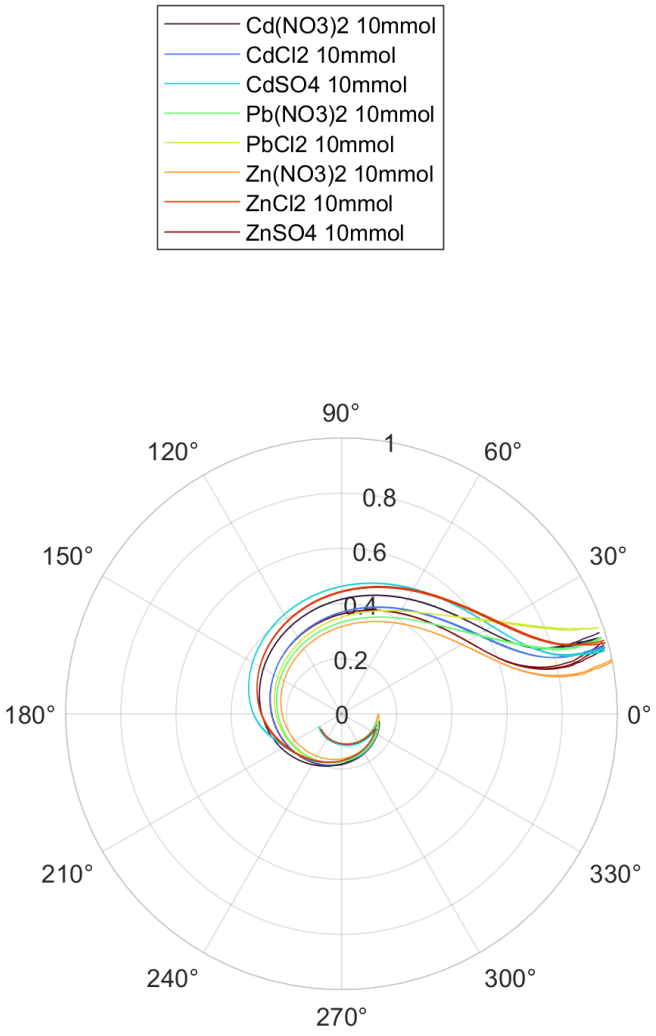

Figure 13 Impedance visualized in polar coordinates for EIS with 10 mmol/l.

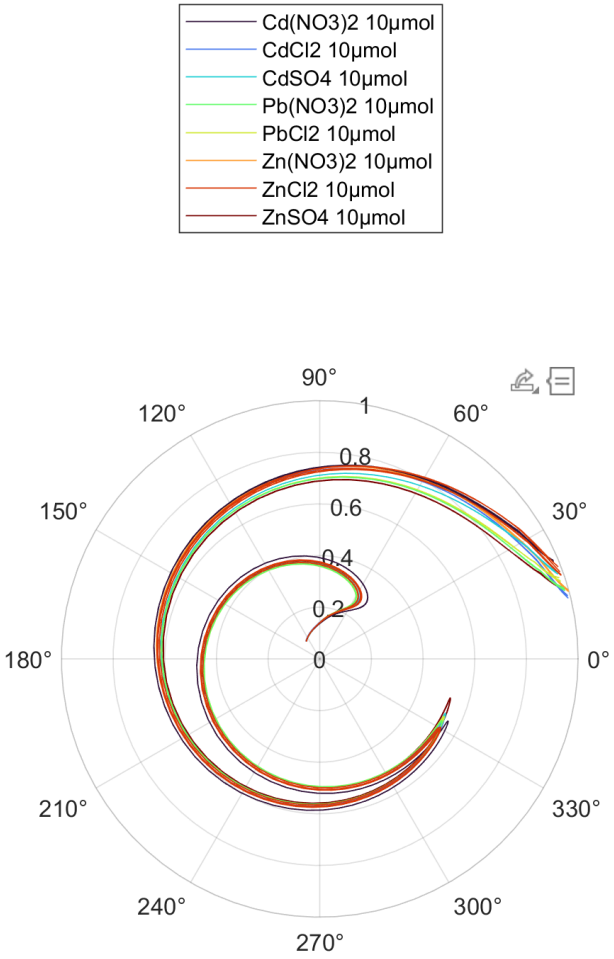

Figure 14 Impedance visualized in polar coordinates for EIS with 10 µmol/l.

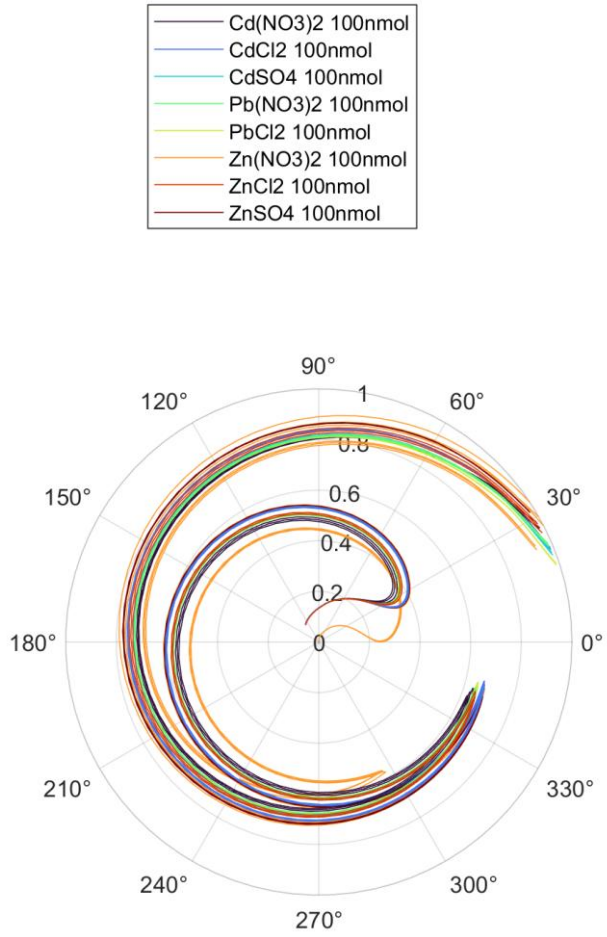

Figure 15 Impedance visualized in polar coordinates for EIS with 100 nmol/l.

3.2 Development of a CNN model to classify solutions

Using the polar visualizations of our EIS measurements, we further developed a convolutional neural network (CNN) model to classify solutions. With 76 samples in total, one-third was reserved for testing purposes, while the remaining two-thirds were used for training and validation purposes.

In this study, the CNN architecture was chosen to explore the EIS measurements, because of its capability to extract features from images. Unlike traditional machine learning models that rely on manually engineered features, CNNs automatically learn hierarchical representations—starting from simple edges and curves in the early layers to more complex patterns in deeper layers. Note that all images were prepared in greyscale and colours were only used to illustrate group characteristics in preceding sections.

For image-based classification of EIS polar plots, we adopted SqueezeNet (Iandola et al., 2016), a lightweight convolutional neural network architecture originally proposed by Iandola et al. (2016) . SqueezeNet achieves an AlexNet-level accuracy with 50× fewer parameters and a model size of less than 0.5 MB, making it highly efficient for efficient deployment on resource-constrained systems (e.g. desktop or laptop-based applications). The core design principle of SqueezeNet is the use of Fire modules, which consist of a squeeze layer (1×1 convolutions) followed by an expand layer (a mix of 1×1 and 3×3 convolutions). Its efficiency is based on three strategies: (1) replacing most 3×3 filters with 1×1 filters to reduce parameter count, (2) reducing input channels using a squeeze layer, and (3) delay downsampling (via pooling) to maintain large activation maps for as long as possible, improving accuracy.

Its layer-by-layer architecture is introduced as follows (Figure 16):

1. Conv1 Layer
    - 96 filters of size 7×7, stride 2 (where stride is the step size by which the convolution or pooling window moves across the input)
    - Followed by ReLU activation (Rectified Linear Unit - An activation function applied after a convolution or fully connected layer) and MaxPooling (3×3, stride 2, A downsampling operation that reduces the spatial dimensions of feature maps.)
    - Purpose: Extract low-level features from the input image.

2. Fire Modules (Core Building Blocks)
    - Each Fire module consists of:
        - Squeeze Layer: 1×1 convolution to reduce channel depth.
        - Expand Layer: Combination of 1×1 and 3×3 convolutions applied to the squeezed output.
    - Fire modules are stacked as follows:
        - Fire2, Fire3 to MaxPooling
        - Fire4, Fire5 to MaxPooling
        - Fire6, Fire7, Fire8 to MaxPooling
    - Purpose: Efficiently learn hierarchical features while minimizing parameters.

3. Conv10 Layer
    - 1×1 convolution producing K feature maps (where K = number of classes).
    - Replaces fully connected layers to reduce parameter count.

4. Global Average Pooling
    - Averages each feature map into a single value.
    - Purpose: Converts spatial feature maps into class scores without dense layers.

5. Softmax Layer
    - Converts class scores into probabilities for classification.

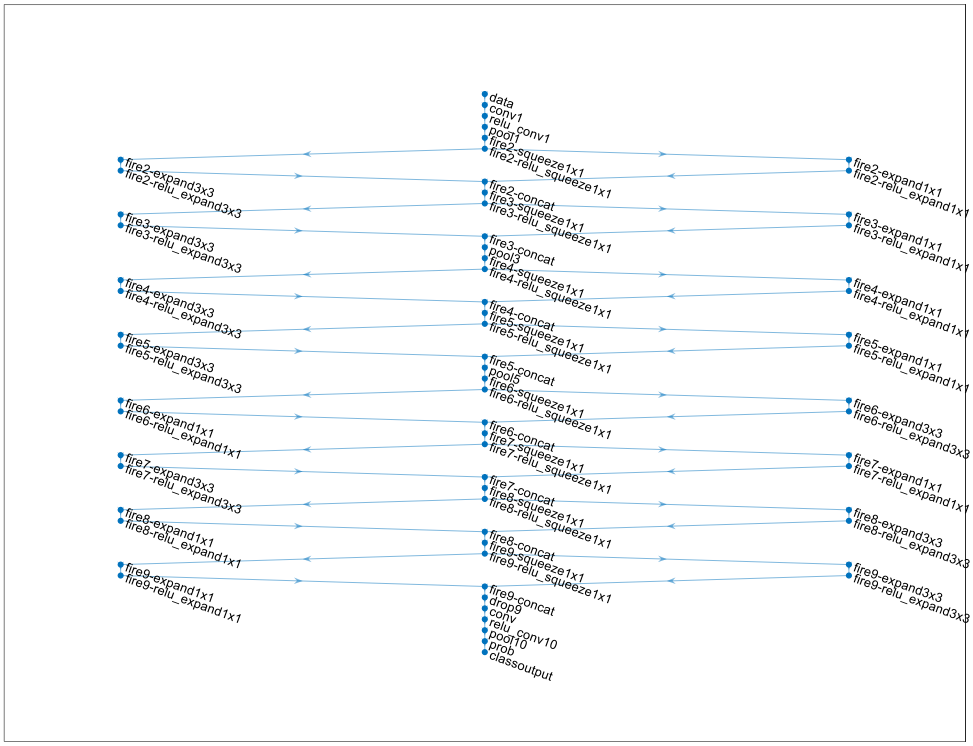

Figure 16 SqueezeNet.

The following (hyper)parameters were used in training the network:

1. **Optimizer:** Stochastic Gradient Descent
2. **ExecutionEnvironment:** Multiple GPUs in parallel for faster training and larger batch handling.
3. **InitialLearnRate: 0.0001,** a small learning rate ensures stable fine-tuning and prevents overshooting.
4. **MaxEpochs: 60,** which is the number of full passes through the training dataset; balances learning and overfitting risk.
5. **MiniBatchSize: 16,** which is the number of images per training iteration; chosen to fit GPU memory while maintaining efficiency.
6. **Shuffle: "every-epoch",** which aims to randomize data order each epoch to improve generalization and prevent memorization.
7. **ValidationFrequency:** 10, which runs validation every 10 iterations to monitor accuracy and detect overfitting early.
8. **TestData:** 1/3 dataset

3.3 Results

Figure 17 presents the classification results for solutions at 10 mmol/l concentration using the SqueezeNet model. The overall accuracy achieved was 95.83%, with 23 out of 24 samples correctly classified. All classes except one were predicted perfectly; the only misclassification occurred when a $Zn(NO_3)_2$ sample was incorrectly labeled as $Cd(NO_3)_2$. This indicates that the model performs very well for most salts at this concentration, but there is some overlap in the spectral features of $Zn(NO_3)_2$ and $Cd(NO_3)_2$, which likely caused the confusion. Despite this single error, the results demonstrate strong discriminative capability of the model for high-concentration solutions, with clear potential for further improvement through additional data and targeted augmentation.

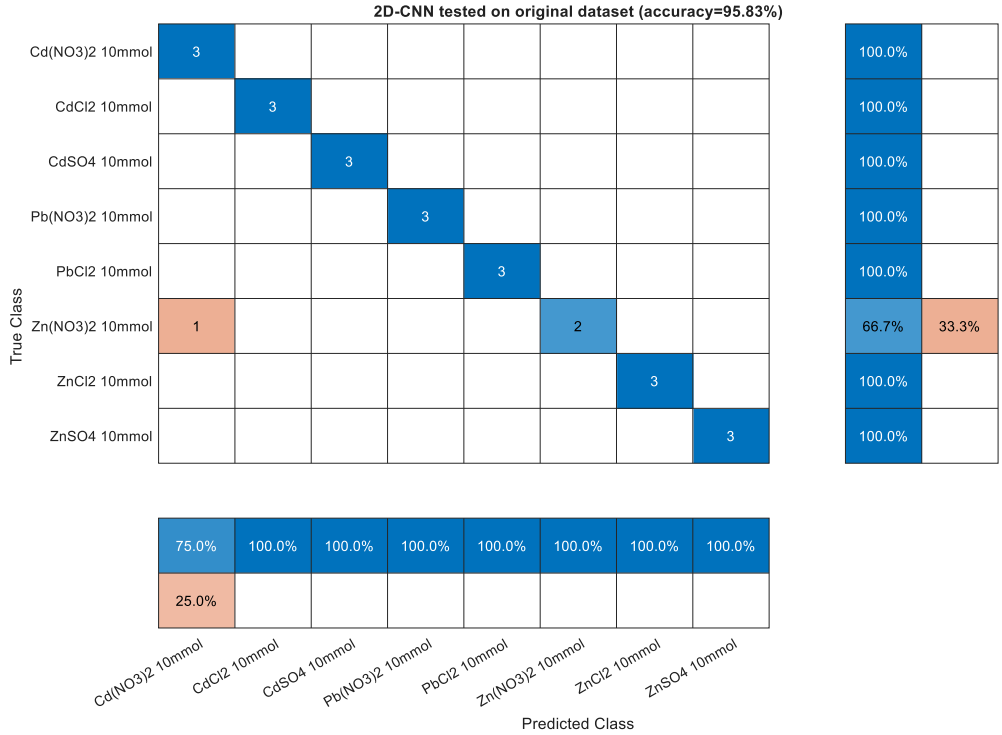

Figure 17 Results for the solution concentrations of 10 mmol/l.

Figure 18 shows the classification results for solutions at 10 µmol/l concentration , achieving an overall accuracy of 96.30%. Out of 27 test samples, only one misclassification occurred: a $Zn(NO_3)_2$ sample was incorrectly predicted as $ZnSO_4$. All other classes, including $CdCl_2$, $CdSO_4$, $Pb(NO_3)_2$, $PbCl_2$, and $ZnCl_2$, were classified with 100% accuracy. This indicates that the model performs extremely well at this intermediate concentration, with strong class separation and minimal confusion.

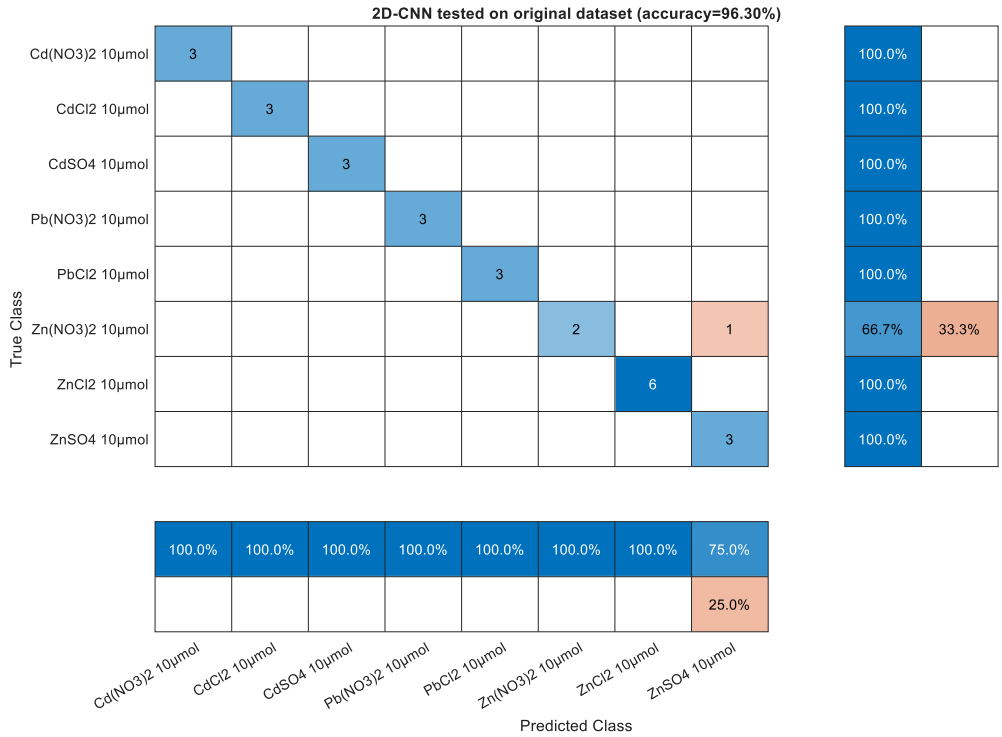

Figure 18 Results for the solution concentrations of 10 µmol/l.

Figure 19 presents the classification results for solutions at 100 nmol/L concentration, where the model achieved an overall accuracy of 92.59%. Out of 27 test samples, two misclassifications occurred: one $Zn(NO_3)_2$ sample and one $ZnCl_2$ sample were incorrectly predicted as other classes. All other classes were classified correctly. These results indicate that while the model still maintains strong performance at very low concentrations, the increased misclassification rate compared to higher concentrations suggests that impedance patterns become less distinct as ionic strength decreases. This highlights the need for combining the classification model with a regression model to predict the concentration of solutions in advance.

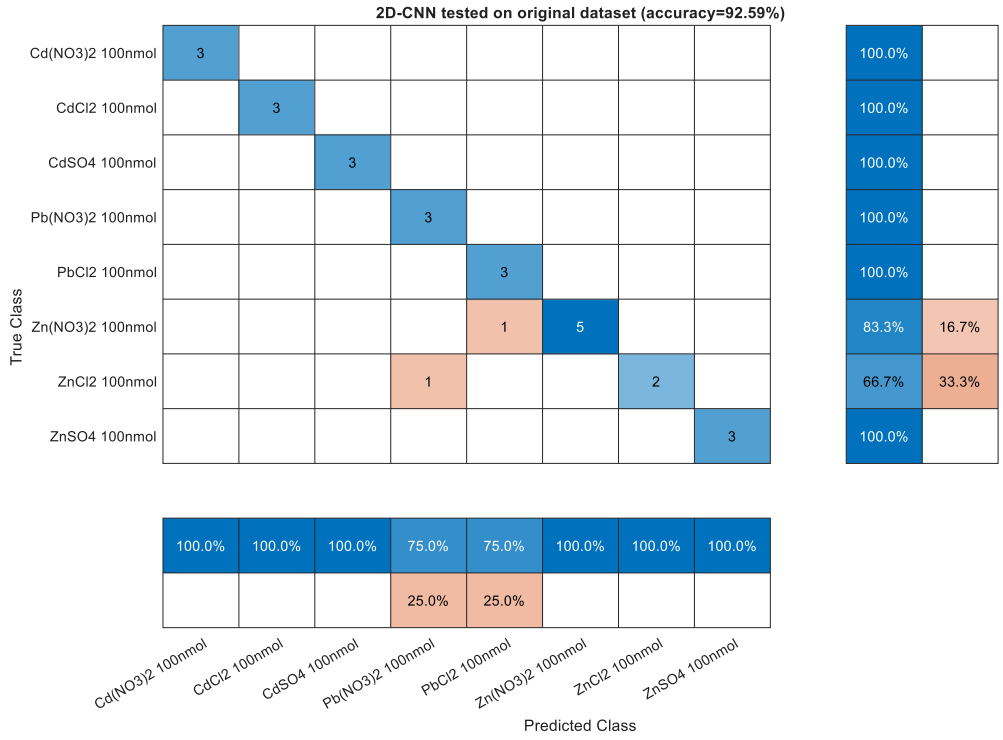

Figure 19 Results for the solution concentrations of 100 nmol/l.

3.4 Concluding remarks and future works

The SqueezeNet model consistently achieved high accuracy across a range of solution concentrations. At 10 mmol/l, the model classified 23 out of 24 samples correctly, reaching an overall accuracy of 95.83%. For the 10 µmol/l concentration, it successfully classified 26 out of 27 samples, resulting in an accuracy of 96.30%. At the lowest concentration tested (100 nmol/l), the model achieved an accuracy of 92.59%, with only two misclassifications out of 27 samples. These results demonstrate the model's ability to distinguish between different salts, even as concentrations vary.

Although the current results are promising, there is still room for improvement—especially at lower concentrations. Enhancing the dataset, applying targeted data augmentation, and integrating the classification approach with regression models to estimate concentration levels beforehand could further boost performance and reliability.

To further enhance model performance and scalability, several improvements are proposed for our future work. First, implement a multi-label classification approach to allowing simultaneous identification of multiple ions within a single sample (instead of the solution), reflecting real-world scenarios where mixed solutions may occur. Second, explore simpler and more lightweight architectures than SqueezeNet, such as custom shallow CNNs or 1D-CNN, to reduce computational complexity and training time without sacrificing accuracy. Third, integrate a concentration prediction model alongside the classification model, enabling the system to more accurately identify the type of solution based on the estimated concentration, given that fact that the low concentration may lead to less accurate classification results.

4 Application of sensor in pilot systems

4.1 Introduction to TUBES

The TUBES facility (Figure 20: TUBES – Picture of the TUBES building.Figure 20 and Figure 21) is designed to serve as an intermediate step for testing new technologies and methods before they are deployed in real, functioning drinking water distribution systems. Located at KWR, TUBES is a compact yet realistic representation of the Dutch drinking water distribution network. It includes over 400 meters of reconfigurable piping in diameters ranging from 80 to 400 mm, constructed from various materials such as ductile iron, PVC, PE, PE-AL, and GFRP (Figure 22). Its maze-like layout features multiple bends, joint types, T-sections, valves, hydrants, and other elements commonly found in operational networks. Powered by three pumps, the facility can handle pressures up to 10 bars and flow speeds exceeding 2 m/s in parts of the network.

TUBES supports the introduction of sediments, bubbles, and solutes into the flow, making it ideal for testing under realistic conditions. It also allows for the incorporation of used pipe sections, adjustable pipe alignments, and even controlled leak simulations. Nearly the entire setup is installed above ground for easy access and modification, and its high level of hydraulic control enables precise experimentation. The facility is supported by a data-centric online architecture, with a Digital Twin currently under development to enable advanced monitoring and remote operation.

TUBES offers real-time monitoring and control of water quality and hydraulics and enables testing of failure scenarios and emergency response strategies in a safe and non-disruptive manner. It uses actual materials and configurations from the field, which makes experiments highly relevant for operational practice. The facility is also used as a training and diagnostics platform, allowing field crews to practise handling realistic network events without affecting live systems.

Another important function of TUBES is its role as a testbed for sensors. Utilities can trial new monitoring technologies, such as pressure sensors, flow meters, and water quality probes, under controlled conditions before rolling them out in the field. Thanks to its modular construction, the layout of the network can be reconfigured with ease, making it possible to test and compare different network types, such as branched and looped systems.

Figure 20: TUBES – Picture of the TUBES building.

Figure 21: TUBES – Pictures of the pipes inside (top) and outside (bottom).

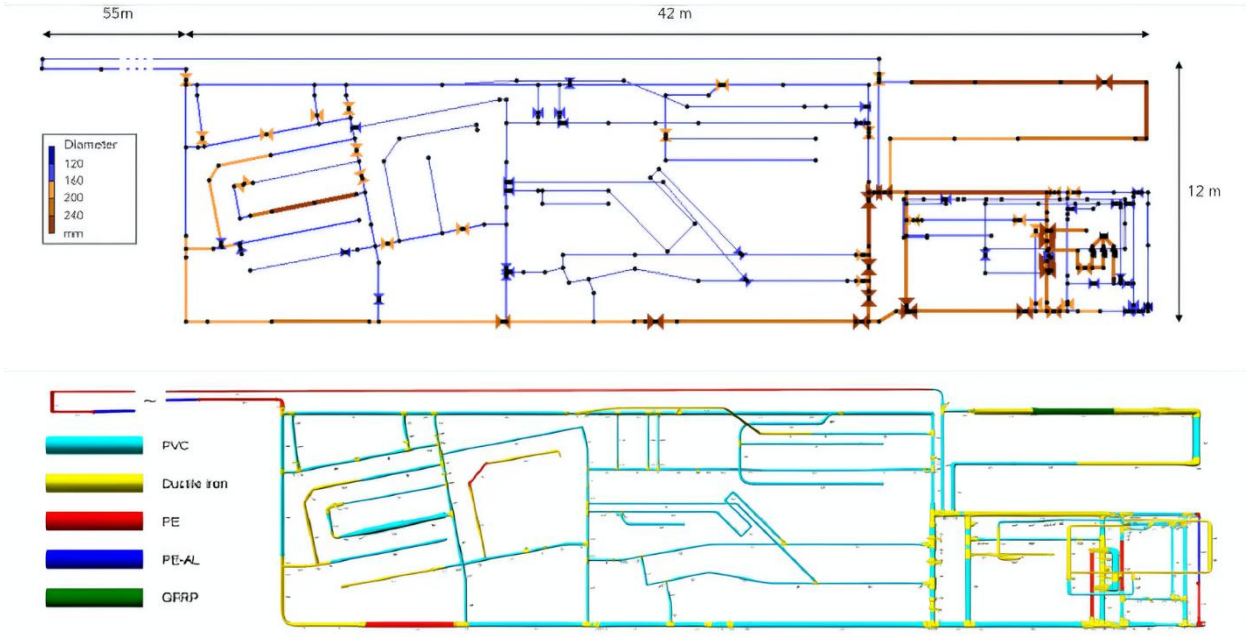

Figure 22: TUBES - System diagram. Top figure shows the diameter of the pipes and the bottom figure shows the type of pipes (material).

4.2 Small test installation

In contrast to the TUBES setup, this installation can only hold a few litres of liquid. It was specifically used to test the sensors in a complex aqueous matrix, which is not feasible with TUBES. The setup consisted of closed-circuit polymer tubing through which liquids were pumped using a close-coupled pump (Figure 23). A storage container is part of the system to increase the volume of the system.

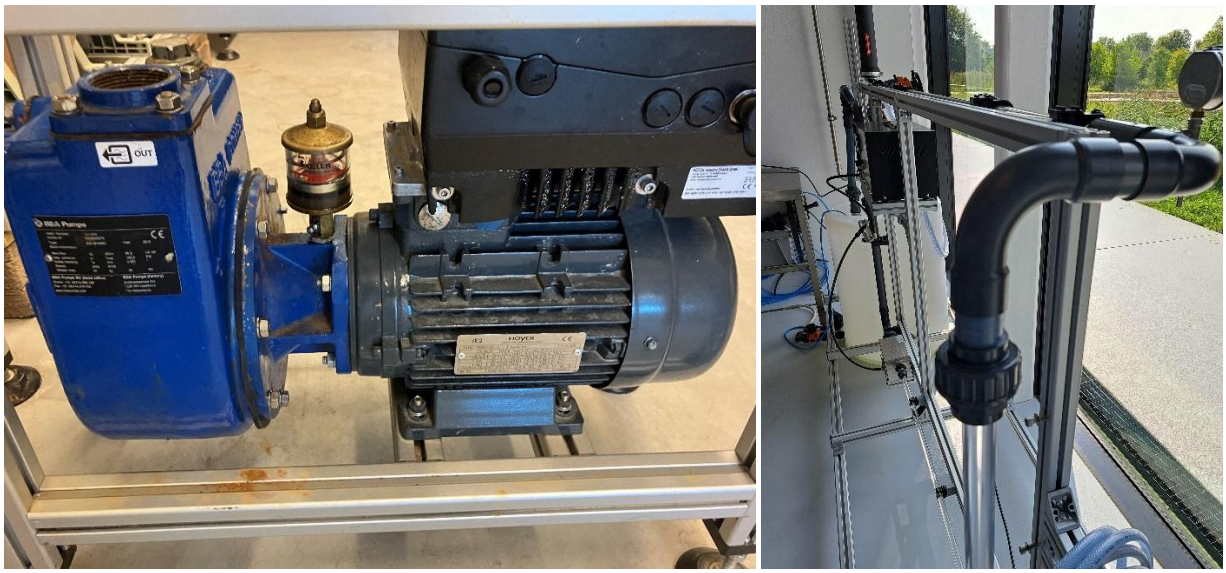

Figure 23: Closed-coupled pump (left) and closed-circuit pipe system (right).

4.3 Robusq sensor and Prototype Alpha

At Hypersoniq, multiple sensor configurations were under development during this TKI project. As the chip sensor was mainly suitable for fundamental studies due its high sensitivity to external noise, another sensor configuration was used for testing in an industrial environment. A three-electrode setup was used with 2 mm diameter circular electrodes, in a configuration called the RobusQ as seen in Figure 24. Three identical electrodes were positioned flush in a plane, ensuring identical distance between the working, counter and reference electrode. Different measurement characteristics were obtained in this sensor configuration as compared to the chip configuration. Initial lab measurements with selected salt solutions and lab proof of concept measurements with industrial samples showed promising results with this sensor setup, meaning the sensor showed comparable results to the lab bench experiments.

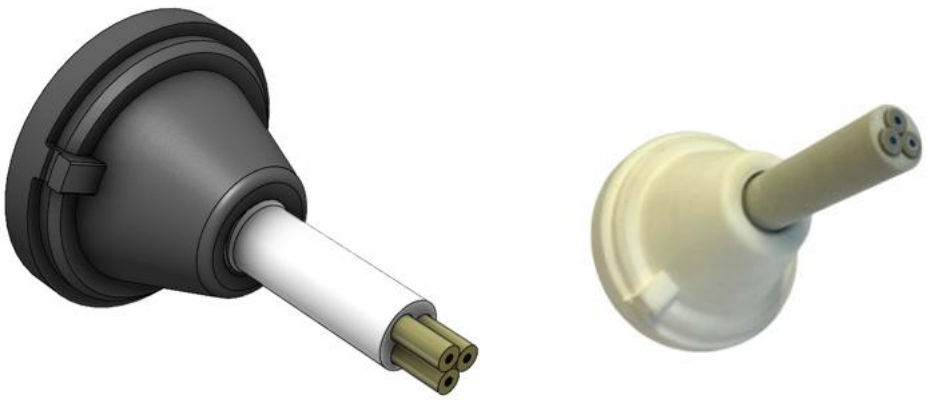

Figure 24: RobusQ sensor

At the same time, an industrial prototype Alpha was designed, engineered and manufactured for testing and application in industrial environments. This prototype was designed to be installed in a bypass configuration on a process line or vessel. The prototype included an automated sampling system, with a hand valve, a pressure regulator, pumps, valves, a pre storage container and a measurement chamber inside a Faraday cage. The system also includes a tank for a cleaning liquid and pumps to perform automated cleaning cycles when needed. Finally, an electrical cabinet housed a PLC, power supply, PC with 4G connection module and auxiliary electronics (Figure 25).

While the measurement method wasn't yet fully developed, the EIS measurements were primarily performed to investigate their stability and at minimum phase shift, the conductivity could be determined to compare to known salt concentrations.

The Prototype was subjected to a validation program with three primary purposes:

1. Validate the EIS measurements performed in the prototype vs. the lab setup
2. Perform basic functional performance tests of the prototype
3. Perform EIS measurements in industrially relevant conditions (@KWR)
    1. Perform basic functional performance test in industrially relevant conditions (TUBES)
    2. Perform a long duration test (TUBES)
    3. Perform measurement in varying feed flow and pressure settings (TUBES)
    4. Test varying additive concentrations (small test installation)
    5. Test in fouling feed (greasy water) conditions (small test installation)

The first two tests were performed at Hypersoniq premises and are not covered in this report. Testing the unit in industrially relevant conditions was done at the TUBES installation and at the small test installation, for which the results are shared here. In the sections above, the industrially relevant conditions are described for the TUBES and small test installation.

Measurement parameters are as follows:

Table 3: Prototype Alpha EIS measurement parameters

Parameter	
Method	1x OCP + 1x EIS
OCP duration	180 s
Frequency range	0,1 Hz – 10^6 Hz (57 frequencies)
E_{dc}	0 V
E_{ac}	10 mV

4.4 Results TUBES

Figure 25: Hypersoniq engineers prepare for the tests

4.4.1 Perform basic functional performance test in industrially relevant conditions

The Prototype was connected to the TUBES system by first drilling a ¾" threaded hole into one of the PVC pipe sections in the short cycle which was located indoors. A hose was attached which led the sample into the Prototype, using the pressure of the liquid in the pipe. A discharge hose was connected to the drain on the floor. After some minor leakages were detected and fixed in the connections inside the Prototype, the first measurement runs were performed successfully. This meant that automated measurements could be performed, and data was successfully sent to the database via 4G. A typical measurement did contain some noise between 1000 Hz and 100.000 Hz, which was also observed when testing the lab, See Figure 26. The source of this noise was not found during the Pre-pilot and still has to be investigated.

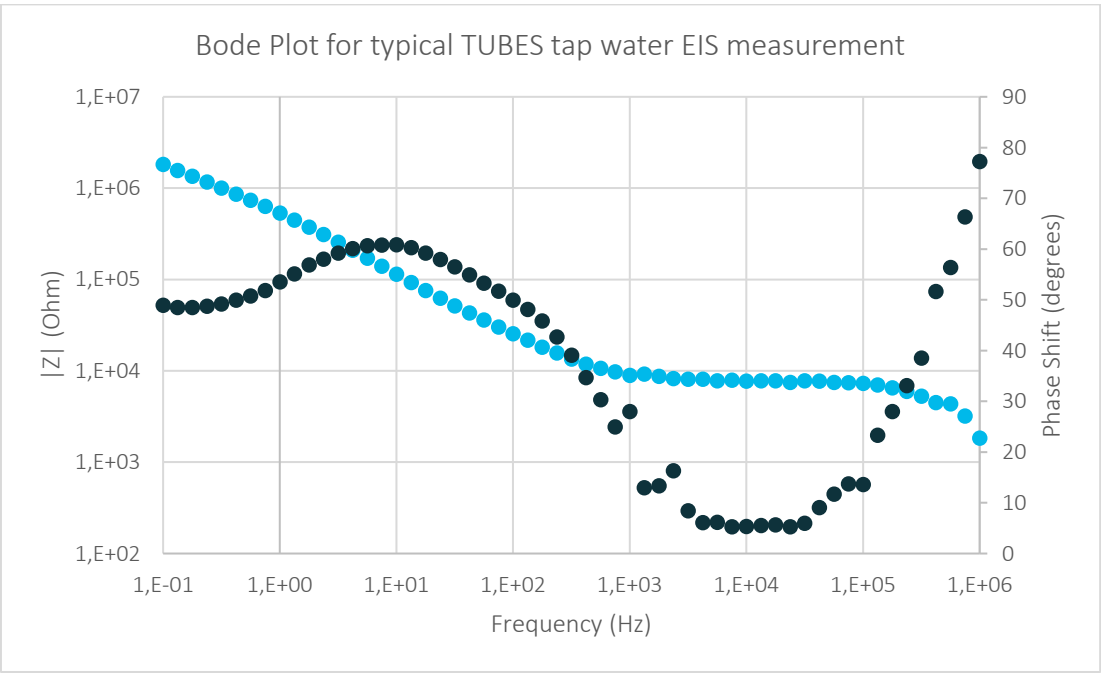

Figure 26: Typical tap water EIS spectrum obtained by Prototype Alpha at TUBES

4.4.2 24-hour long term stability test

Throughout a 24 hour time period from 03-10 at 17:00 until 04-10 at 17:00, approximately 300 measurements were performed. This experiment was performed primarily to assess the stable functioning of the Prototype on a mechanical, hydraulic and connectivity level. No issues were encountered during the full 24-hour period on these aspects, except for very minor leakages at some connections.

When the impedance modulus at minimum phase shift (corresponding to the conductivity) is plotted vs. time, a stable value is obtained as can be seen in Figure 27. There are a few outliers visible, which can be due to random noise. These still need to be investigated.

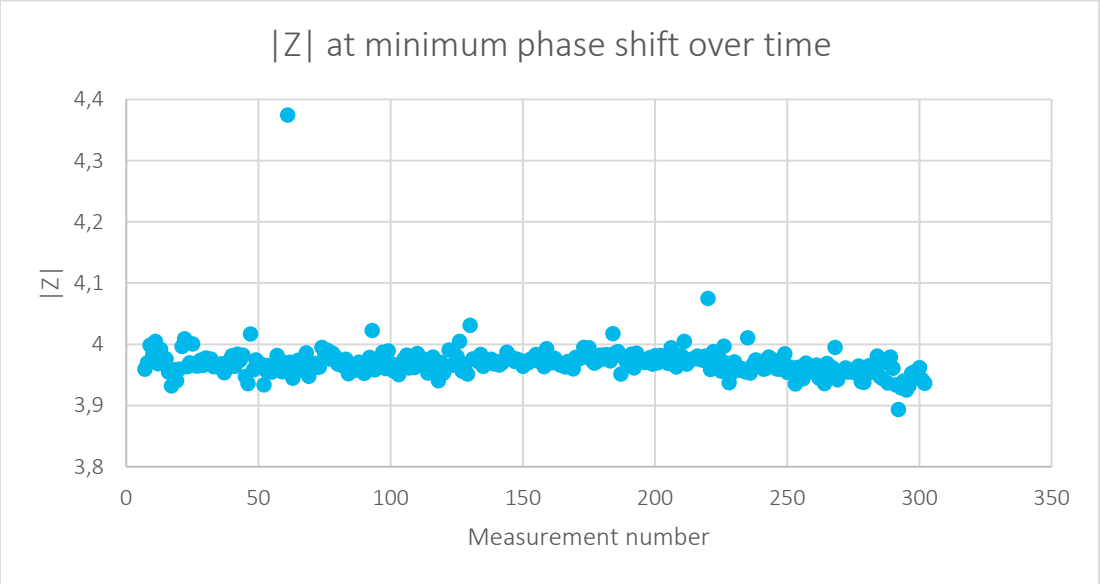

Figure 27 |Z| at minimum phase shift over time during 24 hour long term test

There is a small variation visible over time, which is likely caused by the temperature dropping overnight. If the |Z| values and temperature values measured inside the prototype are plotted over time an inverse relation is visible where resistance increases with decreasing temperature and vice versa, as expected, see Figure 28.

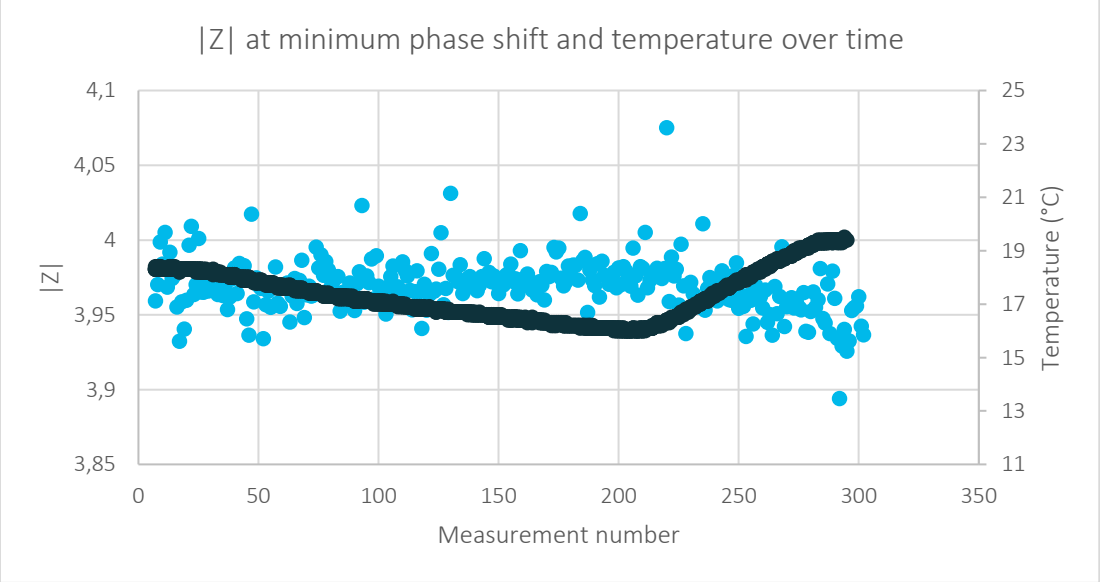

Figure 28 |Z| at minimum phase shift (blue) and temperature (black) vs measurement number.

4.4.3 Test under varying process conditions

To verify that the sampling subsystem of the prototype operated correctly under different process conditions, the flow and pressure were systematically varied over the course of a programmed sequence. The primary goal of these tests was to identify hydraulic integrity of the system and whether the correct amount of sample was collected in the pre-storage tank and measurement chamber.

Table 4: Pre-storage tank level and observations at varying process conditions

	Pressure in supply pipeline (Barg)	Flowrate (m^3/h)	Pre-storage tank level (mm) (after filling, before pumping)	Observations
04-10-2024	0.8	x	x	Successful in 24-hour test. Minor leakage at filter connections
09-10 11:25	1.07	23.2	22	Still minor leakage at filter connections
09-10 12:01	2.05	26.5	30	Pressure ramp up started at 12:01, took until 12:05 to stabilize at P and F levels
09-10 13:00	2.54	26.4	30	Pressure ramp up started at 12:57. At 13:00 first measurement was started. P and F data as here to the left.
09-10 13:23	2.44	30.2	31	No additional leakage, stable performance
09-10 13:52	2.5	50.0	30	No additional leakage, stable performance
09-10 14:09	2.0	91.9	31	No additional leakage, stable performance

The most important finding is that even at increased pressure levels of up to 2,5 Bar (maximum value in the TUBES system) there was a stable level in the pre-storage tank, and no additional leakage was observed in the connections. Also at increasing flowrates, pre-storage tank level was stable. The flowrate and pre-storage data at lowest pressure and flow were not registered.

Figure 29: Hypersoniq engineers troubleshooting under the watchful eye of KWR staff

4.5 Results of small test installation

4.5.1 Varying salt concentrations

At the time of testing with the RobusQ electrode setup, the lab tests had shown strong correlation between impedance measurements at minimum phase shift and conductivity measurements performed with a commercial sensor. This can be expected from theory as conductivity is inversely related to resistance, and at minimum phase shift the capacitive contribution is minimal. The current test phase focused on measuring varying KNO_3 concentrations in the small test installation at KWR. KNO_3 was chosen as a model salt, because it is safe and easy to handle. This experiment served to test the sample volume required for flushing to obtain a representative measurement in the sample chamber. After an iterative approach it was found that flushing 1,5 L of sample was needed. A sequence of increasing KNO_3 concentrations was created by adding solution to the system's main tank, followed by a series of dilutions achieved by partially draining the tank and refilling it with tap water. Throughout this procedure, the prototype continuously sampled and measured the solution. Salt additions were recorded and conductivity was measured using a handheld commercial sensor to validate the results, see **Error! Reference source not found.**. Temperature was recorded at each concentration level to evaluate its impact. Temperatures remained remarkably stable.

Table 5:Varying salt concentration results

Concentration KNO_3 in system after change (g/l)	Conductivity measured (µS/cm)	Average temperature (°C)	Tap water conductivity (µS/cm)	|Z| at minimum phase shift (log_{10} Ω)
0.450	1134	19.7	288	3.33
1.339	1895	19.7	288	3.25
2.205	2570	19.7	288	3.09
3.050	3190	19.7	288	2.92
3.874	3780	19.7	288	2.78
4.677	4340	19.7	288	2.70
3.937	4160	19.7	288	2.72
3.196	3670	19.7	288	2.78
2.471	3080	19.7	288	2.88
1.760	2200	19.7	288	2.98
1.017	1649	19.7	288	3.26

When the measured |Z| and the KNO_3 concentrations are plotted, a negative correlation is obtained which shows that EIS measurements with the RobusQ electrode setup in the prototype can be used to measure salt concentrations.

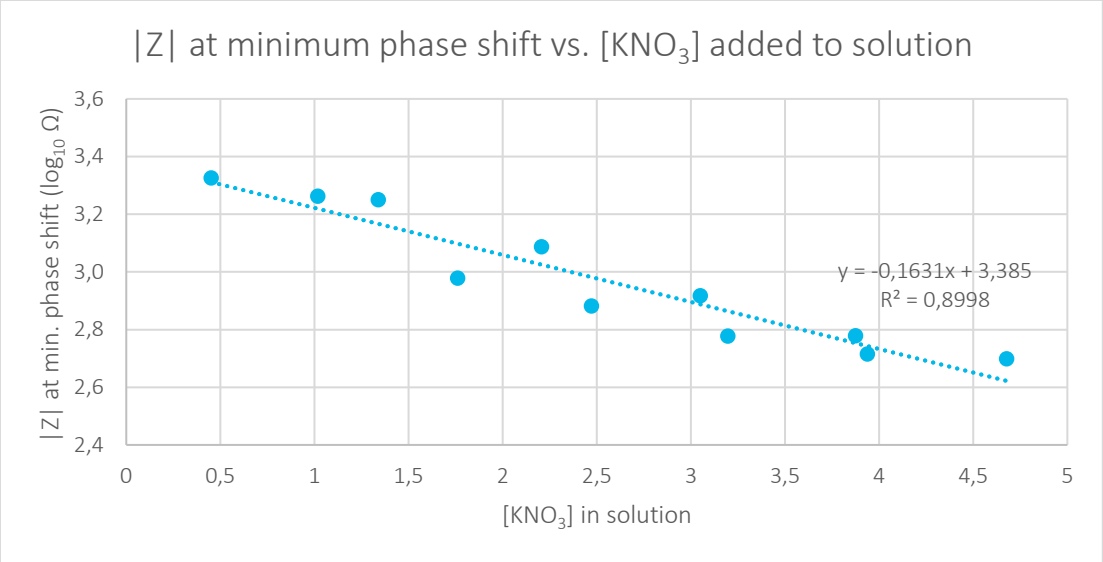

Figure 30: |Z| plotted against the concentration of KNO_3.

4.5.2 Test in water with a high fat content

To validate that the prototype still functions as required in fouling feed conditions, a real-life wastewater sample was obtained from a ready to eat meal factory. Normally, this wastewater has Chemical oxygen demand (COD) levels of up to 12.000 mg/L, contains significant amounts of suspended solids, and fats, oils and grease. This wastewater was added to the small-scale test setup at KWR and circulated, while measurements were performed with the prototype. All components such as valves, couplings and tanks functioned as required and measurements were performed normally over the course of around one hour, while 15 EIS measurements were performed. No significant change was observed in the measured EIS spectra over this time, although surface fouling of the electrodes was observed as can be seen in Figure 31. The fouling mechanism, how fouling affects the measurements, and possible cleaning methods are to be investigated after this pre-piloting phase.

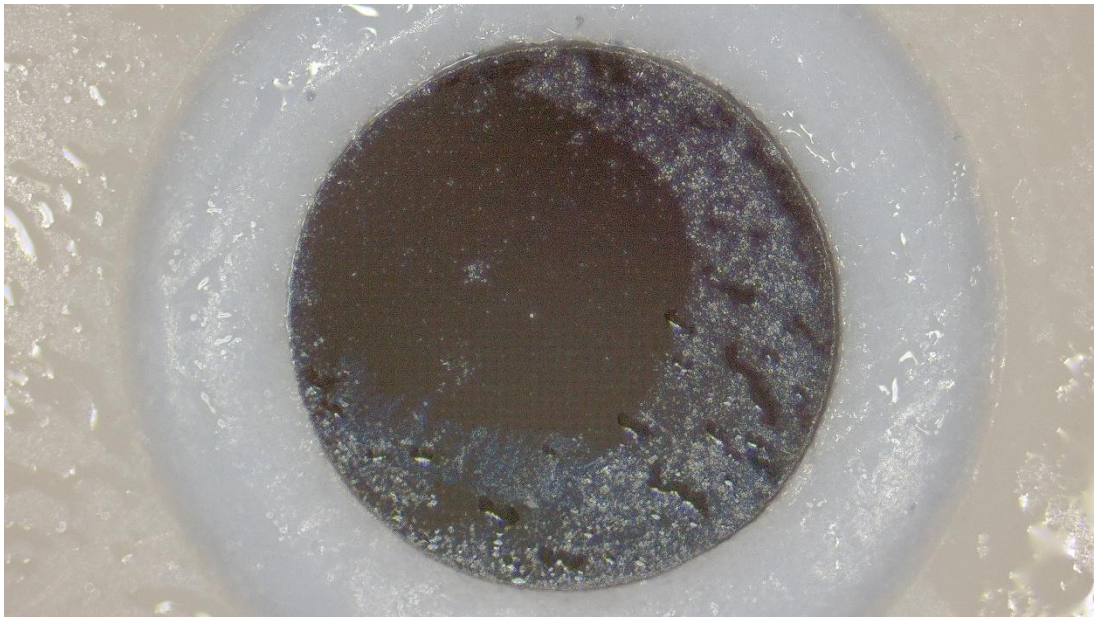

Figure 31: Graphite electrode microscope image after exposure to industrial wastewater sample

5 EIS to determine particle size

5.1 Earlier research

An earlier study by Zhang *et al.* found the use of electrical impedance spectroscopy (EIS) as a new method to measure the structure and size of particle aggregates, such as sludge flocs, during water and wastewater treatment processes (Zhang et al., 2022). Traditionally, techniques like light scattering or microscopy are used to assess the properties of sludge flocs. However, these detection techniques come with limitations—for example, they can be sensitive to the colour of the sample or require time-consuming sample preparation. EIS is a non-invasive and low-cost technique that offers the possibility of real-time, and in-situ measurements, and is not sensitive to colour. By adjusting the particle concentration, they could relate the electrical signal to overall structural characteristics. Changing the frequency of the electrical field, enabled detecting features within individual flocs, such as their internal structure and size. To make this work, they created a mathematical framework linking EIS data to two key properties: the fractal dimension, which describes the complexity or density of particle structures, and floc size, which they estimated by identifying a characteristic change in the impedance signal known as 'the critical frequency'. The method was tested on various systems, including activated sludge from wastewater treatment plants, synthetic colloids and gels, and a real-world sludge pre-treatment process using potassium permanganate. The results showed that the method could accurately detect changes in particle structure and size. There was a strong correlation between the EIS signals and actual particle size, confirming that EIS could be used as a reliable indicator. In the practical sludge treatment test, the method successfully detected the optimal oxidation time to improve sludge dewaterability. Additionally, the fractal dimensions calculated using EIS aligned well with those obtained from established techniques like light scattering and confocal microscopy. This study shows that EIS is a promising tool for online monitoring of particle size and structure in water treatment systems. It overcomes many of the limitations of traditional methods and performs well even in coloured or complex samples. Because of its advantages, this approach offers potential for more intelligent process control in wastewater treatment, encourages further research into the role of aggregate structure, and could be applied more broadly across different treatment scenarios.

In this study we investigated if EIS measurements can be used to determine the size of particles in surface water suspensions as well as in suspension made in the laboratory.

5.2 Sensor and calibration

Conductivity cell TetraCon® 325/C was bought from Xylem and connected to a PalmSens SP-200 (Houten, The Netherlands). The connection setup was verified by performing an EIS measurement on a 0.01 molar KCl solution (mol/kg), which has a known electrolytic conductivity (κ) of 1.273 mS/cm at 20 °C. Using the measured conductivity (G) of 2.71 mS, the cell constant (k, in cm^{-1}) was calculated as k=κ/Gk = \kappa / Gk=κ/G, resulting in a value of 0.47 cm^{-1}—matching the cell constant specified in the sensor manual (0.475 cm^{-1}).

5.3 Size measurement of carboxylated polystyrene nanoparticles

A solution of 20mM NaCl was prepared. Additionally, carboxylated polystyrene (PS) beads with a diameter of 520 nm were suspended in said 20 mM NaCl: Two particle concentrations were prepared: 7×10^6 and 1.82×10^8 particles per mL. Of these three solutions the Nyquist plots were acquired (Figure 32).

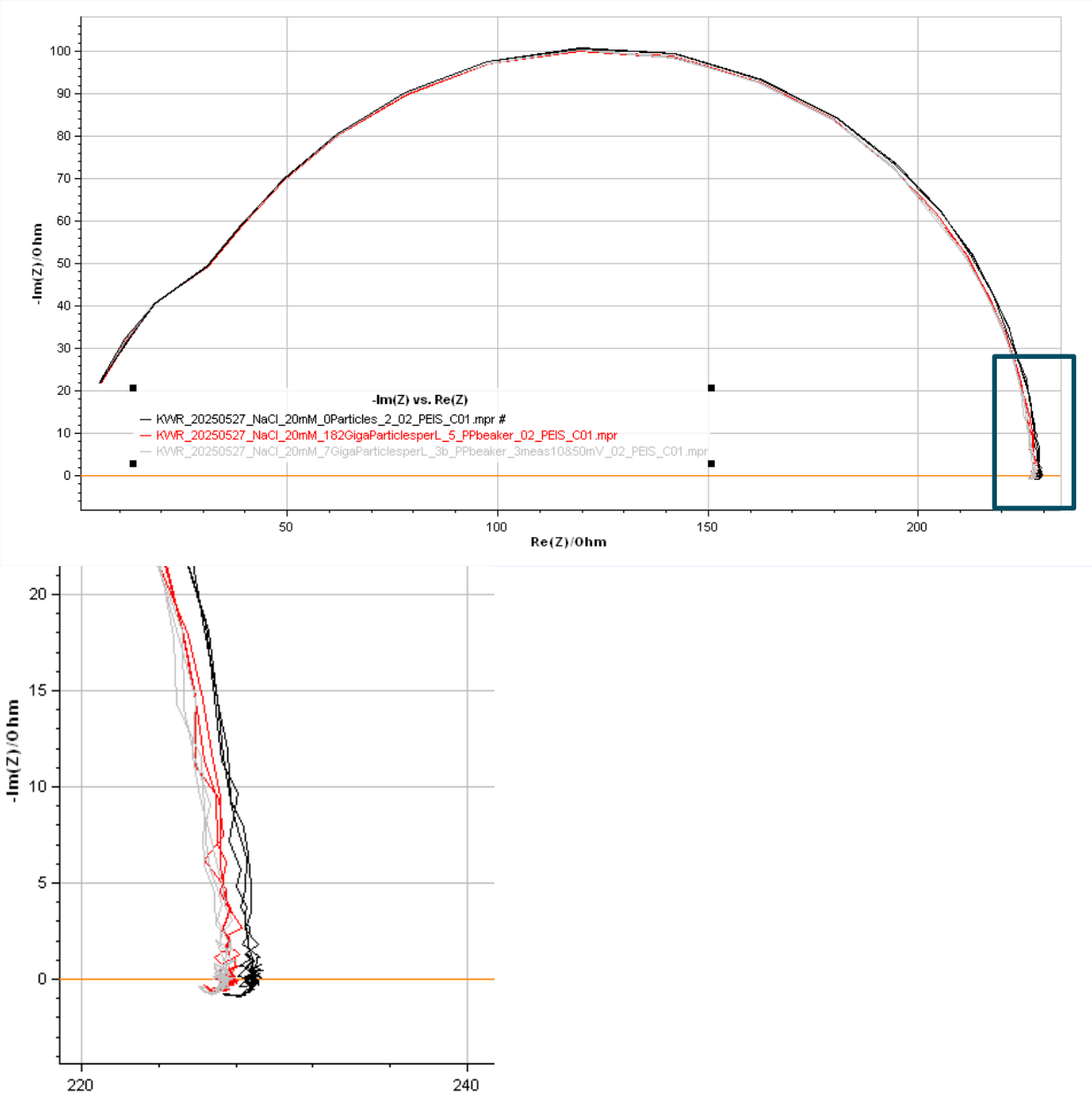

Figure 32: Nyquist plot of 20 mM NaCl solution (black), 20 mM NaCl solution with 7 × 10^6 particles per litre (grey) and 20 mM NaCl solution with 1.82 × 10^8 particles per litre (red).

For each solution a different signal is acquired. However, there is no clear tendency. The solution with the highest particle count has as Re(Z) value in between the pure NaCl solution and the solution with the lowest particle number. Also, the differences in the recorded signals are minor. These minor variations could also be attributed either to temperature fluctuations, uptake of CO_2 or to slight differences in NaCl concentration. It is known that slight changes in temperature can cause such a shift. Therefore, this data does not show any effect of the particles on the impedance signal. With the applied test setup, we were not able to detect the concentrations of carboxylate polystyrene particles at the selected concentration range.

5.4 Size measurement of citrate capped silver nanoparticles

Three suspensions containing silver nanoparticles were prepared. For the 80 nm citrate-stabilized silver nanoparticles, two concentrations were made: 7.6×10^7 and 1.5×10^8 particles mL^{-1} in 20 mM NaCl. In addition, a suspension of 40 nm citrate-stabilized silver nanoparticles was prepared at a concentration of 1.1×10^9 particles mL^{-1} in 20 mM NaCl. Nyquist plots were subsequently acquired for all suspensions (Figure 33).

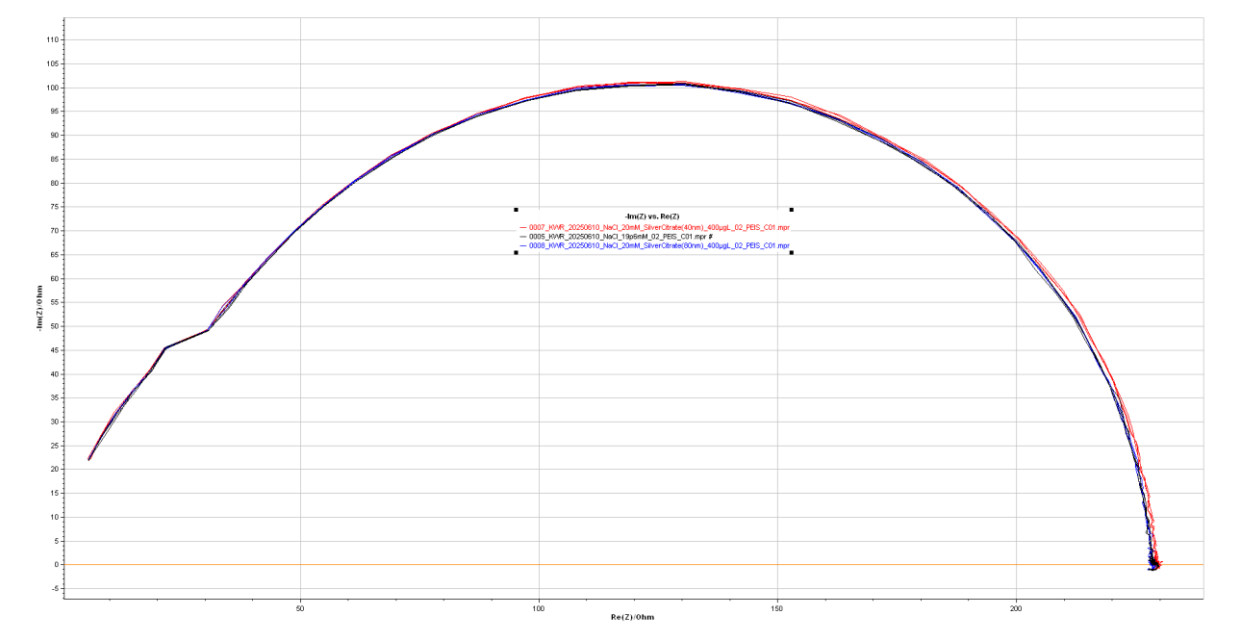

Figure 33: Nyquist plot of 19.6 mM NaCl solution (black), 40 nm particles 400 µg/L in 19.6 mM NaCl solution (red), 80 nm particles 400 µg/L in 19.6 mM NaCl solution (blue).

There is no noteworthy difference between the three Nyquist plots meaning that based on this data nor the size nor the concentration of the nanoparticles can be measured at the given concentration and size range.

5.5 Size measurement of naturally present particles in water from the Lek canal

To determine if with EIS measurements, the size of micrometre sized particles can be determined, a surface water suspension was collected. The sample, taken from the Canal Lek (Lekkanaal), was measured before and after sequential filtration through 45 µm, 20 µm, and 10 µm filters, without applying vacuum filtration. Measurements were conducted in a 600 mL glass beaker containing a 4 cm magnetic Teflon stir bar, using a stirring apparatus enclosed within a Faraday cage. The stirring rate was set to 190 rpm and maintained throughout the measurements. Previous testes showed no difference in EIS results between stirred and unstirred conditions. Particle size distribution was determined using a PAMAS Waterviewer HCB-LD-50/50, with the stirring rate during sample recirculation set to 200 rpm (Figure 34).

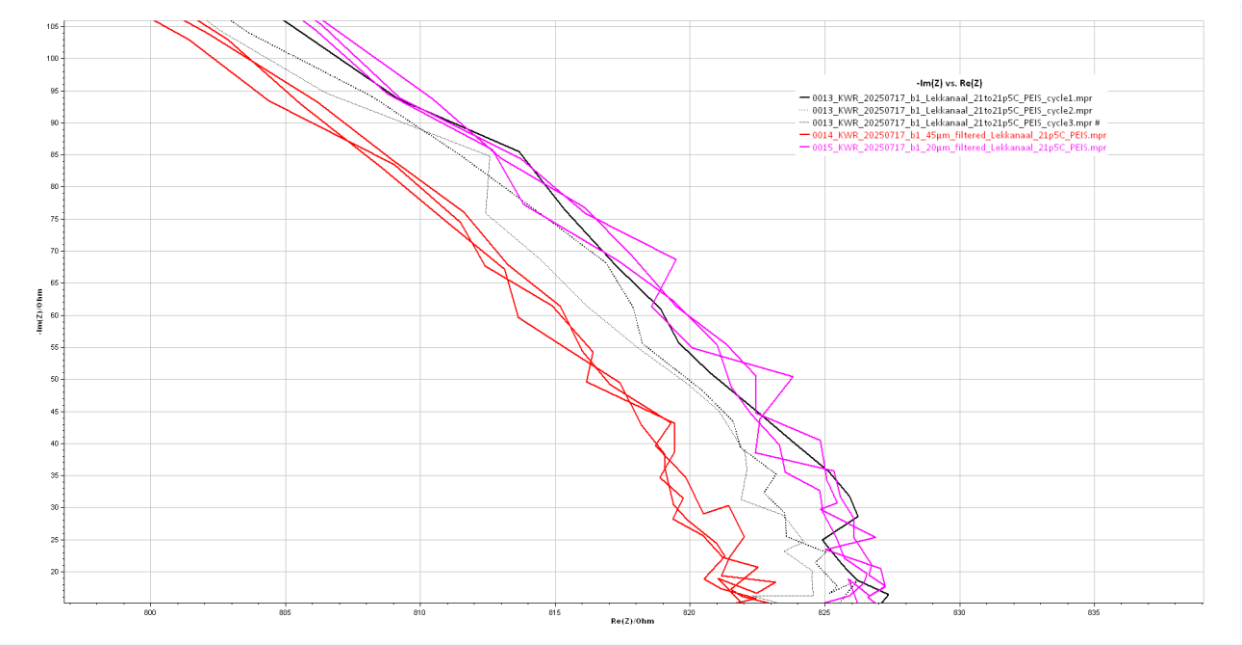

Figure 34: EIS measurements of Lekkanaal water before and after filtration at varying temperatures. Black solid line: unfiltered water at 21.0 °C; Black dashed line: unfiltered water during temperature increase from 21.0 to 21.5 °C; Black dotted line: unfiltered water at 21.5 °C. These three curves represent a single measurement with three cycles as the temperature increased. Red line: sample filtered over 45 µm at 21.5 °C; Pink line: sample filtered over 20 µm at 21.5 °C.

Figure 34 shows the scattering profiles of Lekkanaal water under different conditions. The black solid line represents the unfiltered water measured at 21.0 °C, while the black dashed line corresponds to intermediate measurements as the temperature increased from 21.0 °C to 21.5 °C. The black dotted line marks the final state at 21.5 °C. These three curves together correspond to a single measurement with three cycles, during which the temperature gradually rose from 21.0 °C to 21.5 °C.

The red curve shows the same water sample after filtration through a 45 µm filter at 21.5 °C. Compared to the unfiltered sample (black dotted), this curve is shifted to the left, indicating a change due to removal of larger particulates. However, in contrast, the pink curve, representing the water filtered through a 20 µm filter at 21.5 °C, is shifted to the right of the unfiltered solution. It seems counterintuitive that if more particles are removed (using a filter with a smaller mesh size) the signal should shift in the opposite direction.

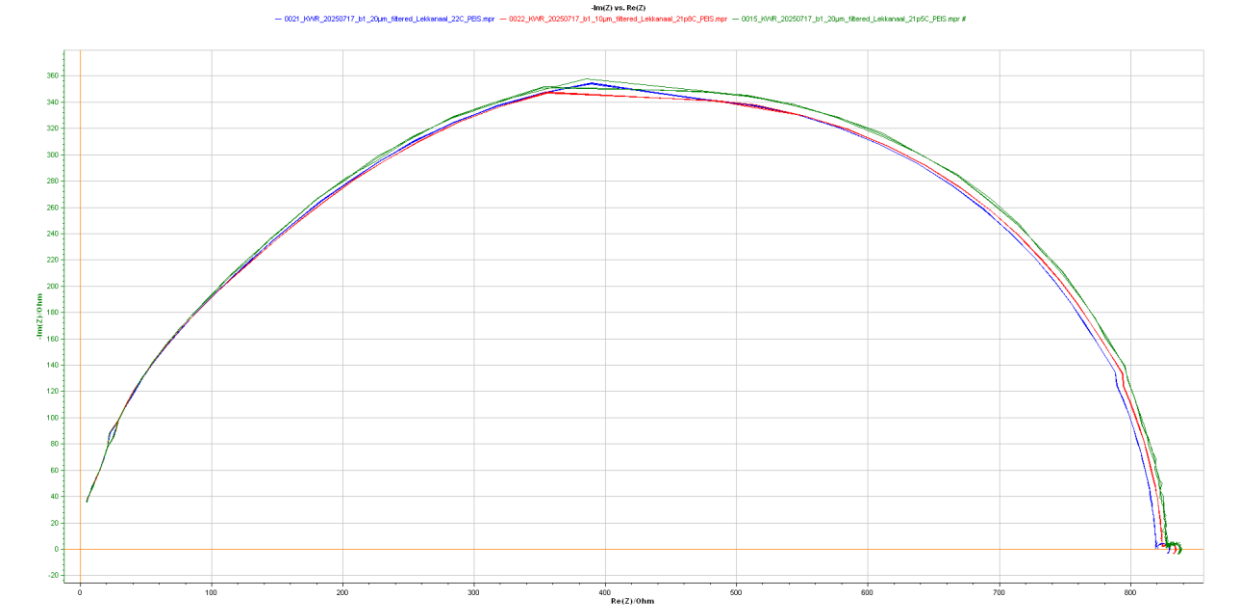

Figure 35: EIS measurements of Lekkanaal water filtered over different pore sizes and measured at varying times and temperatures. Green line: water filtered over 20 µm at 21.5 °C (measured at 11:06); Blue line: the same 20 µm filtered sample measured 2.5 hours later at 22.0 °C (measured at 13:34); Red line: water filtered over 10 µm at 21.5 °C.

Figure 35 shows the scattering behaviour of Lekkanaal water after sequential filtration. The green curve represents the water filtered over 20 µm and measured at 21.5 °C. After 2.5 hours and an increase of 0.5 °C (measured at 22.0 °C), the same 20 µm filtered solution is shown in blue, which is shifted to the left compared to the initial (green) curve. These slight temperature differences are unintentional and cannot not be prevented in the current set up. The red curve corresponds to the sample filtered over 10 µm and measured at 21.5 °C. This curve falls between the green and blue curves. While the comparison between the green (20 µm, 21.5 °C) and red (10 µm, 21.5 °C) curves suggests some differences, the more pronounced shift is observed between the green and blue curves of the same 20 µm filtered solution, indicating that time and temperature changes have a greater impact on the scattering profile than the particle concentration.

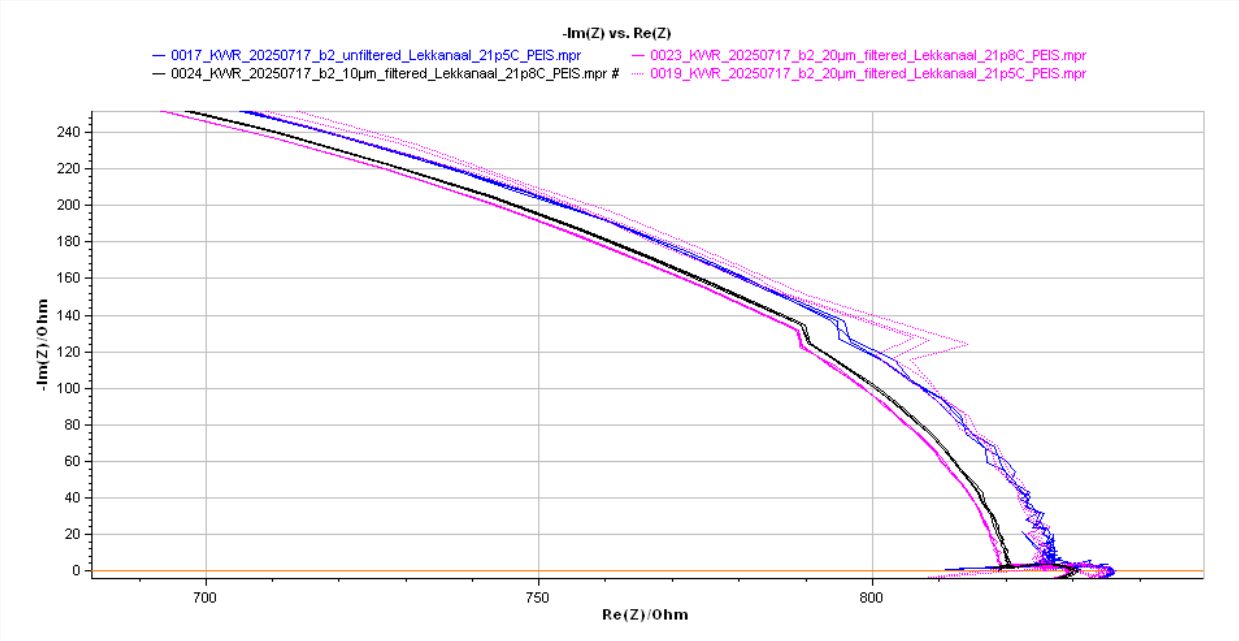

Figure 36: EIS measurements of Lekkanaal water before and after filtration at different temperatures and times. Blue line: unfiltered water at 21.5 °C; Pink dotted line: filtered over 20 µm at 21.5 °C (measured at 12:11); Pink solid line: same 20 µm filtered sample measured later at 21.8 °C (measured at 13:59); Black solid line: water filtered over 10 µm, measured at 21.8 °C (same temperature as pink solid).

Figure 36 shows scattering profiles of Lekkanaal water. The blue curve represents the unfiltered water measured at 21.5 °C. The pink dotted line corresponds to the same water filtered over 20 µm and measured at 21.5 °C, while the pink solid line shows the same 20 µm filtered solution after 1.8 hours and at a slightly higher temperature of 21.8 °C.

The black solid line represents the water filtered over 10 µm and measured at the same temperature (21.8 °C) as the pink solid curve. A comparison between the pink dotted and pink solid lines indicates that temperature has a more pronounced effect on the scattering profile than filtration alone. While a measurable difference is observed between the 20 µm and 10 µm filtered solutions at the same temperature, it remains relatively small. A more substantial difference in particle size or concentration could yield a more pronounced effect, but this would require maintaining constant temperature conditions, which is not possible within the current setup.

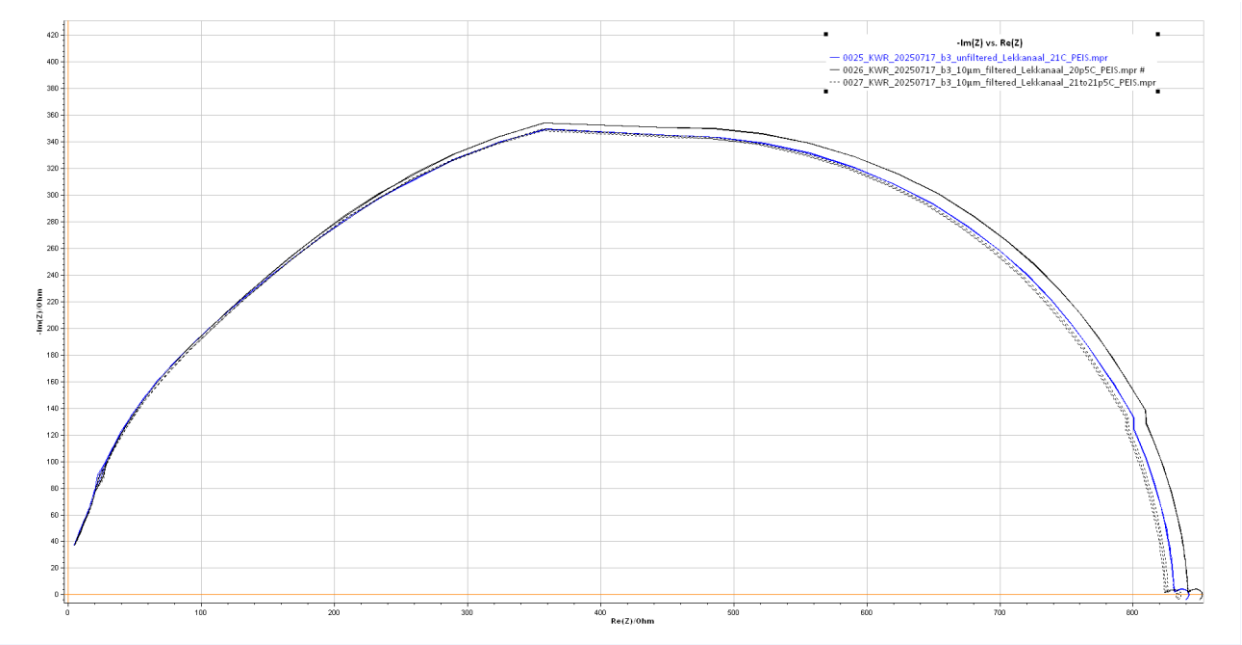

Figure 37: EIS measurements of Lekkanaal water before and after filtration, and the effect of temperature. Blue line: unfiltered water at 21.0 °C; Black solid line: water filtered over 10 µm, measured at 20.5 °C; Black dashed line: same sample as black, measured during warming from 21.0 to 21.5 °C—showing a leftward shift in the curve with increasing temperature.

Figure 37 shows the scattering profiles of Lekkanaal water before and after filtration and the effect of temperature on the filtered sample. The blue curve corresponds to the unfiltered sample measured at 21.0 °C. The black solid line represents the water filtered over 10 µm and measured at a slightly lower temperature of 20.5 °C. The black dashed line illustrates the temperature dependence of the filtered sample as it warms from 21.0 °C to 21.5 °C, resulting in a leftward shift of the scattering curve. The dashed and black line both show measurements at 21 °C, yet they do no coincide although seemingly all parameters are the same.

In addition to the EIS measurements, particle concentrations were determined using a particle counter (Figure 38 to Figure 40), with particles categorized into eight size-windows. These measurements were done to ensure that there were actual differences between the different suspensions. The suspensions were analysed unfiltered and filtered through a 10 µm filter. As expected, particles equal to or larger than 10 µm were effectively removed or significantly reduced after filtration. Interestingly, however, the number of smaller particles increased following filtration. This unexpected rise may be due to the fragmentation of larger particles during the filtration process. This observation could help explain why the EIS measurements showed no clear difference before and after filtration.

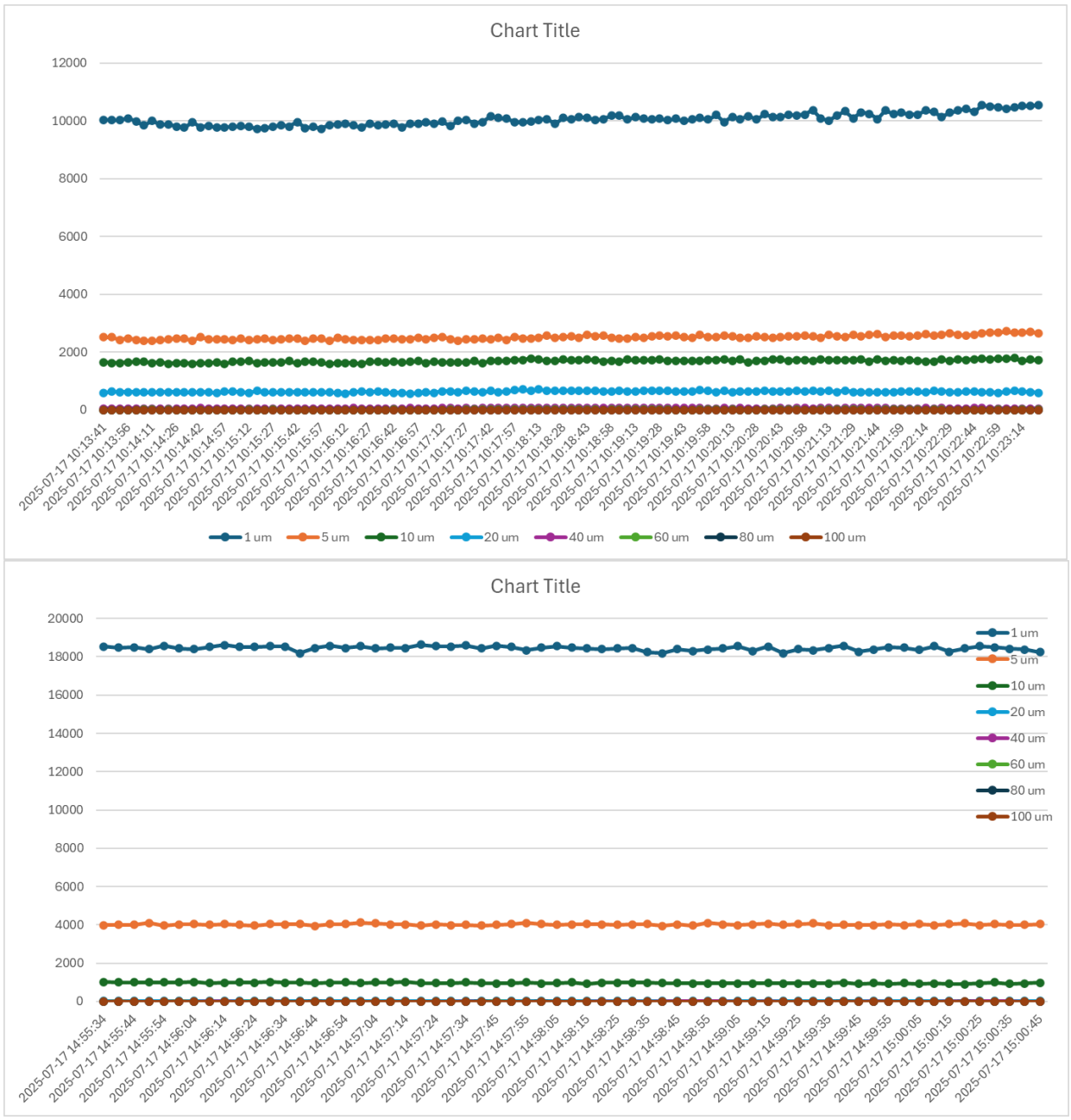

Figure 38: Particle count Lek canal unfiltered (top) and filtered (bottom) through 10 µm.

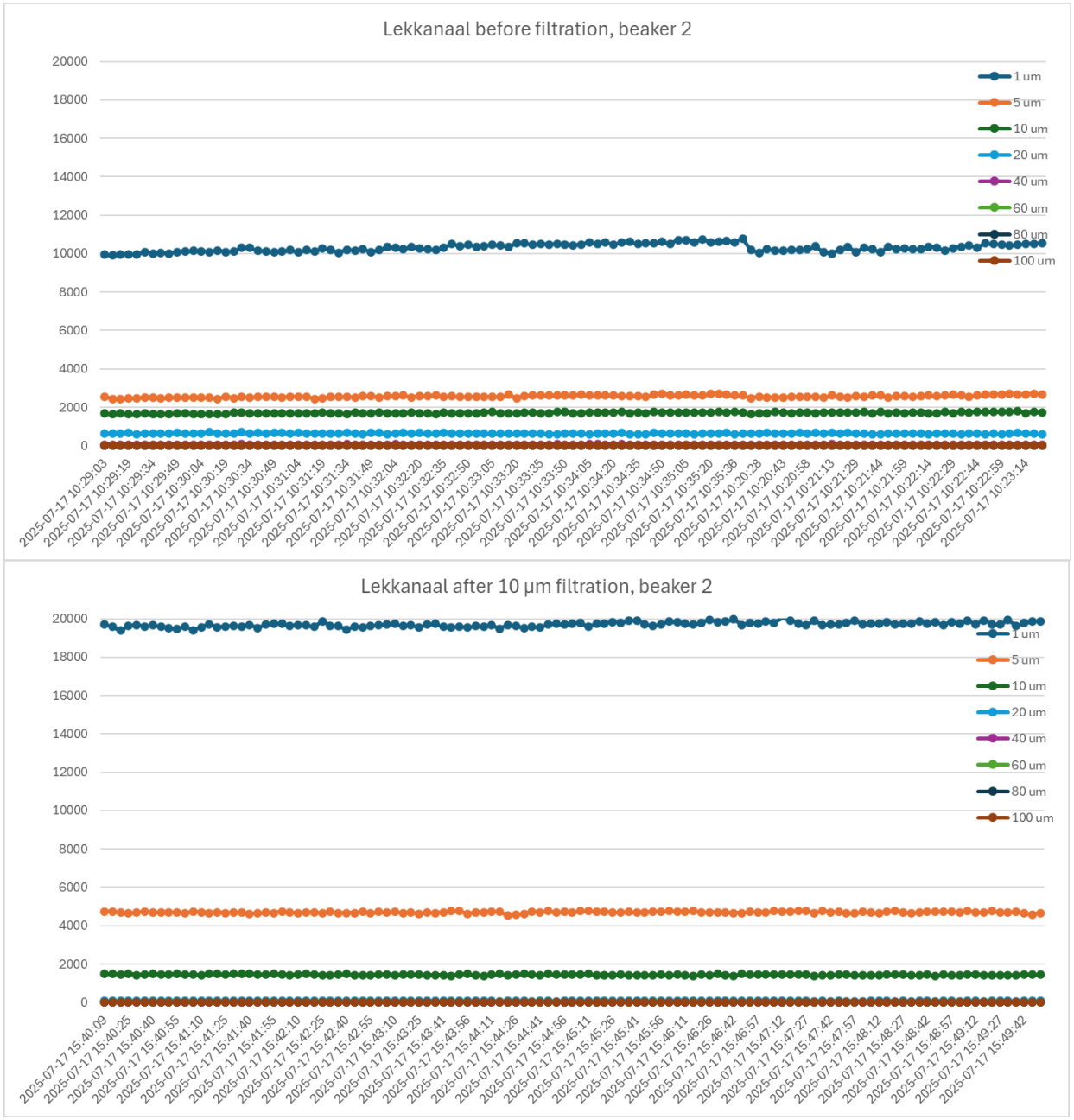

Figure 39: Particle count Lek canal unfiltered (top) and filtered (bottom) through 10 µm.

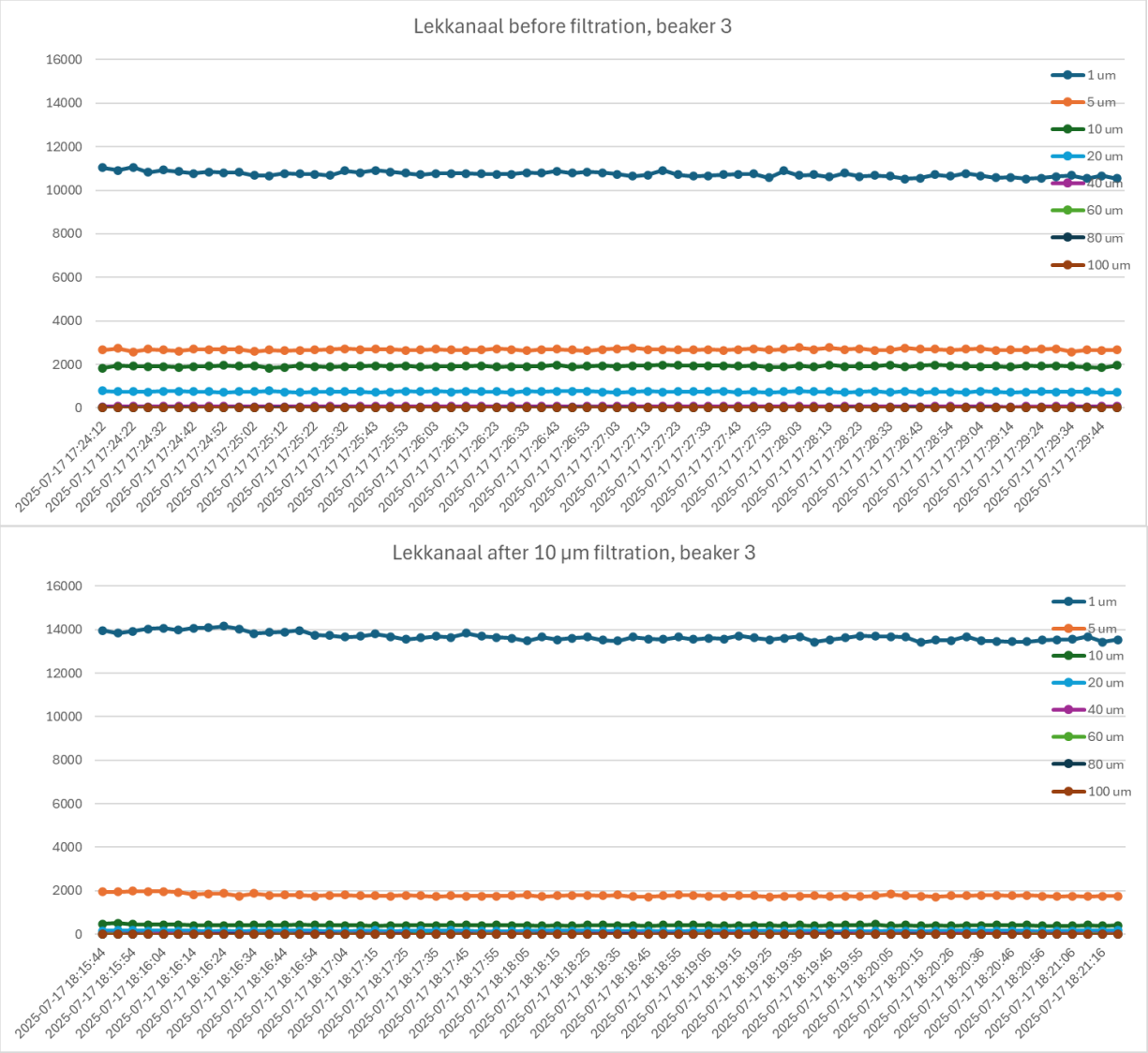

Figure 40: Particle count Lek canal unfiltered (top) and filtered (bottom) through 10 µm..

5.6 Conclusion

Based on the results, a discernible effect of particle size or concentration cannot be measured. There might be an effect, but this effect is overshadowed by other parameters that change during measurement, such as the temperature, CO_2 uptake and particles breaking apart. To evaluate if EIS is indeed a promising technique for particle characterisation and quantification the experiments need to be conducted under more controlled conditions. However, if effects like temperature change are seemingly that strong, then the usefulness of EIS measurements in industrials settings can be doubted, unless measure are taken to externally control temperatures of tested (batch) samples.

6 Conclusion and suggestions

Various organic and inorganic contaminants were evaluated in this project. Early experiments showed that organic chemicals could not yet be measured reliably, primarily due to sensor contamination and sensitivity limitations. Since these issues could not be resolved within the project timeframe, subsequent work focused on inorganic contaminants. Bench-scale experiments using the developed EIS sensors demonstrated that single inorganic salts as well as mixtures could be analysed successfully. In combination with machine-learning models, the sensor was capable of identifying individual inorganic ions and estimating their concentrations within defined concentration ranges. These results indicate that the sensor has strong potential for monitoring changes in inorganic salt composition.

To verify the bench-scale findings, the sensor was installed in an inline sampler connected to two pilot drinking water distribution systems: one large-scale setup (several cubic metres of water) and one small-scale setup (several litres). The large-scale installation was used to assess whether the sensor could operate reliably under realistic hydraulic and environmental conditions such as pressure fluctuations and temperature changes. The small-scale installation enabled controlled adjustments of salt concentrations, which would not be feasible in the large-scale system. The goal of these experiments was to determine whether the sensor could function under typical operational conditions (flow, pressures up to 2.5 bar) and perform unsupervised measurements over extended periods. The results showed stable performance in both systems. In the large-scale setup, the sensor signal remained consistent over a 24-hour period, with only minor variations likely caused by temperature changes. In the small-scale setup, the sensor clearly detected changes in KNO_3 concentrations.

In parallel, we investigated whether the sensor could be used to determine particle size in suspensions. Although the literature indicates that comparable EIS-based systems may be capable of particle-size assessment, our own experiments did not support this. Even slight variations in temperature, CO_2 concentration, or other matrix conditions caused noticeable changes in the impedance signal, overshadowing any potential effect of particle size. If particle size can be determined using EIS at all, its influence appears too weak compared to these environmental effects.

For future research, it is recommended to focus on inorganic salts, as the sensor has already demonstrated reliable performance in this area. Further evaluation of its performance under real-world installation conditions is, however, necessary to assess its practical applicability. Additionally, given the sensor’s strong capability for ion identification, its integration and application following ion chromatography should be further investigated.

Literature

Choi, W., Shin, H.-C., Kim, J.M., Choi, J.-Y. and Yoon, W.-S. 2020. Modeling and Applications of Electrochemical Impedance Spectroscopy (EIS) for Lithium-ion Batteries. J. Electrochem. Sci. Technol 11(1), 1-13.

Futscher, M.H., Gangishetty, M.K., Congreve, D.N. and Ehrler, B. 2020. Quantifying mobile ions and electronic defects in perovskite-based devices with temperature-dependent capacitance measurements: Frequency vs time domain. The Journal of Chemical Physics 152(4).

Iandola, F.N., Han, S., Moskewicz, M.W., Ashraf, K., Dally, W.J. and Keutzer, K. 2016. SqueezeNet: AlexNet-level accuracy with 50x fewer parameters and <0.5 MB model size. arXiv.

Lazanas, A.C. and Prodromidis, M.I. 2023. Electrochemical Impedance Spectroscopy–A Tutorial. ACS Measurement Science Au 3(3), 162-193.

Mauritz, K. Dielectric_responses. Dielectric_responses.svg (ed), https://commons.wikimedia.org/wiki/File:Dielectric_responses.svg and https://web.archive.org/web/20120204055232/http://www.psrc.usm.edu/mauritz/dilect.html.

Schwarzenbach, R.P., Escher, B.I., Fenner, K., Hofstetter, T.B., Johnson, C.A., von Gunten, U. and Wehrli, B. 2006. The Challenge of Micropollutants in Aquatic Systems. Science 313(5790), 1072-1077.

Zago, M. and Casalegno, A. 2017. Physically-based impedance modeling of the negative electrode in All-Vanadium Redox Flow Batteries: insight into mass transport issues. Electrochimica Acta 248, 505-517.

Zhang, D., Wang, Y., Li, J., Fan, X., Li, E., Dong, S., Yin, W., Wang, D. and Shi, B. 2022. Electrical impedance spectroscopy as a potential tool to investigate the structure and size of aggregates during water and wastewater treatment. Journal of Colloid and Interface Science 606, 500-509.

Supplementary information - Sensor types

I.I Most common sensor types used in online water quality monitoring

pH

The pH value is a measure for the acidity or basicity of a sample, not the reactivity or concentration of single substances; it is impossible to link (changes in) pH to the changes in concentrations of single acids or bases. pH is mainly monitored using potentiometric measurements, i.e. the gain or loss of H+ and OH- ions is measured using an ion selective electrode.

pH sensors are the most widely used water quality sensors in drinking water production processes. pH is primarily used as process control parameter at treatment plants, e.g. to ensure optimal performance for pH dependent treatment processes (coagulation, chlorination). pH is less suited for the detection of general water quality changes or contamination events, as it responds to a limited sub-set of substances. The amount of maintenance depends on the application, the sensor must be calibrated and cleaned regularly if a high accuracy level is required.

Electrical conductivity

Electrical conductivity (EC) is a measure for the capability of a liquid to conduct an electrical current. The conducting behaviour is the result of the ions dissolved in the liquid. All ionic species are measured with EC, but the response of the sensor depends on properties of the ions (charge, ion size) and their dissociation. Therefore it is a general indicator for total ion concentration and not a concentration measurement.

Electrical conductivity sensors are the most robust sensors available today for water quality monitoring. EC sensors are solid state sensors that measure the current through the sample resulting from an alternating voltage applied to two or four electrodes. EC sensors are used in many industrial applications (including ultra-pure water) and in environmental monitoring to determine the concentrations of total dissolved solids (salts). An EC sensor is only able to detect ionic species, and cannot identify individual substances. However, it can be used to measure salt intrusion, which is possible due to the elevated NaCl concentrations, which are much higher than other ions.

Dissolved oxygen (DO)

Modern dissolved oxygen (DO) sensors are mainly of the optical luminescence type, which are robust and have a high stability. A DO sensor measures the saturation of a solution with dissolved oxygen gas. In combination with measurement of temperature, this saturation can be converted into an oxygen concentration. Optical sensors require very little maintenance and deliver results fast (in seconds). DO sensors are the most widely used sensors for process control at wastewater treatment plants.

Turbidity

Turbidity sensors are widely applied and give a measure for the particle load in water. Turbidity measurements are based on the scattering of light that is caused by the particles in the sample (also referred to as nephelometry). The amount of scattered light is measured (e.g. at a 90° angle) and converted into a turbidity value. This value doesn't reflect the number of particles or the nature of the particles and is sensitive to air bubbles in water. Besides the nephelometric turbidity sensors, which are particularly suited for low particle concentrations, sensors are used to measure the concentration of suspended solids. These sensors measure the amount of light absorbed by the matrix, typically using a near infrared light source. This measurement principle relies on a linear relationship of absorbance with the particle load. These sensors are particularly used for high solids concentrations, where the nephelometric measurement would provide insufficient measurement signal. Turbidity sensors are widely used in drinking water treatment and environmental monitoring. Suspended solids sensors are primarily used in the wastewater domain.

Ion selective electrodes

Ion selective electrodes are able to measure specific ions such as Cl^-, F^-, Na^+, K^+, Ca^{2+}, NH_4^+ and NO_3^- in aqueous samples. This technique involves potentiometric measurements to determine the total concentration of the target ion, with selectivity being determined by the properties of the ion selective membrane in combination with electrode materials. Ion selective electrodes require intensive maintenance, in particular frequent calibration, and their linear range is limited. Ion selective electrodes are primarily used in wastewater treatment (NO_3^-, NH_4^+) and environmental monitoring (Cl^-, NH_4^+ and NO_3^-).

Oxidation-reduction potential

Oxidation-reduction potential (ORP) sensors measure the redox potential of a medium, which can be used to determine the relative electron transfer capacity of a solution. Redox reactions are complex and often involve more than one substance, and the ORP of a solution is determined by the sum of all redox active species. ORP is an activity measurement, not a measurement of concentration. ORP sensors are electrochemical devices equipped with an inert electrode in combination with a reference electrode. ORP is a relative measurement; the value depends on the material of the electrode in the sensor, the configuration of the electrode and the physical state of the electrode (ageing, fouling, etc.).

ORP measurements are used primarily to measure reactivity in water, for example to estimate the disinfection potential, showing the activity of the disinfectant instead of the applied dose. ORP is not well suited for monitoring general quality changes and for detection of contamination events, as it only responds to redox active species. Its use is further limited by the difficulty of comparing results between sensors (not consistent), due to the dependence of the measurement results on the layout of the sensor and the state of the sensor. Strong interference from the matrix and the fact that they are difficult to calibrate under field conditions further hamper the successful application of ORP as a parameter for water quality monitoring.

UV/Vis absorbance

A widely used technique in water quality monitoring is online UV/Vis spectroscopy. This technique measures the absorbance at wavelengths in the UV-visible light range. Several device types exist, ranging from monitoring only one wavelength (for example 254 nm) or the whole UV/Vis spectrum. Sensors can be flow through systems or probes submersed in the matrix. The sensitivity of the sensor is defined by the optical path length. A device with a longer optical path length is more sensitive but has a lower maximum concentration. A major disadvantage of UV/Vis spectroscopy is that compounds that do not absorb UV and/or visible light are not detected by the sensor. Moreover, this technique is not very specific, and identification of individual substances is challenging and often impossible. However, some compounds such as BTEX, ozone, phenol, hydrogen sulphide and iron have a strong characteristic absorption which allows identification. The technique is mostly suitable for the determination of sum organic parameters, TOC (total organic carbon), BOD (biological oxygen demand) and COD (chemical oxygen demand). Furthermore, the UV/Vis spectrum provides a fingerprint of the composition of the water and can be used to detect water quality incidents based on deviations in the fingerprint. UV/Vis sensors are solid-state instruments, and require little maintenance, the prime concern being the fouling of the optical windows.

Fluorescence

Another optical technique is fluorescence spectroscopy, which measures emitted photons (usually in the visible range). This technique is primarily used for the monitoring of algae (detection of chlorophyll) and cyanobacteria (detection of phycocyanin). Fluorescence spectroscopy can also be used to detect aromatic substances, thus making it the most commonly used sensor type for measuring oil in water. However, in case the oils have a low aromatic content (vegetable oils, crude oil, gas oil), they cannot be measured using fluorescence spectroscopy. Fluorescence measurements are highly specific for the target substance. Being solid state sensors, they are robust, requiring only little maintenance.

Wet chemical sensors

Wet chemistry analysers are devices designed to perform a traditional wet chemical method fully automated and autonomously. Whereas many sensors (e.g. UV/Vis, fluorescence, ion selective electrodes) are used for online monitoring, their results are not often used for compliance monitoring. As their methods deviate from recognized standard methods, they need to be demonstrated to be able to fulfil, for example, the EU Drinking Water Directive criteria. Currently, the process of equivalence testing is complicated and expensive, and member states do not always accept the results from tests done in another country. The wet chemical analyser provides the user with the option for on-site measurement of chemicals according to the standard methods. Although they are fully automated, these analysers are not very suitable for online water quality monitoring as their operation is costly and requires frequent maintenance. Their use is therefore limited to situations where the information they provide has a direct benefit (process control, in particular in industrial water and water treatment) or where there is a specific obligation for monitoring substances for which no other technology is available. Typical parameters that can be measured include metal ions, silica, phosphate, hydrazine, and COD (chemical oxygen demand).

I.II Sensor types with potential for online water quality monitoring

IR absorbance

In infrared spectroscopy, molecular vibrations can be characterized by measuring the infrared absorbance or transmittance of a sample. Near infrared spectroscopy (NIR) is mainly applied for non-aqueous matrices. NIR is a suitable technique for the analysis of simple mixtures and quality control where known spectra are compared with measured spectra. The technique is not very suitable for the online identification of unknown compounds.

Raman spectroscopy

Raman spectroscopy is a technique which measures the scattering of photons by a molecule. This technique is quite selective but less suitable for identification of compounds in water samples, since these might be too complex mixtures. Raman spectroscopy has higher detection limits than for example UV/Vis spectroscopy but is more selective.

Refractive index

If the composition of a water sample changes, its refractive index changes as well. The refractive index is defined as an optical property describing the propagation of light through a medium. It is a suitable technique for the monitoring of stable matrices (such as drinking water) and to detect whether anything is out of the norm, since this will cause a change in refractive index. However, this technique is not suitable to identify the cause of the deviation.

Cyclic voltammetry

Sensors based on cyclic voltammetry measure the current at the working electrode whilst a varying (cycling) potential is applied between the working electrode and the reference electrode. By selecting the electrode materials and the voltammetric profile this technology can be used to measures specific metal ions. Applications are found in the measurement of lead, cadmium, nickel and zinc. Although the method is applied in laboratories, with the dropping mercury electrode being one of the oldest electrochemical analytical methods, its use under field conditions remains largely limited to experimental and research applications.

Molecularly Imprinted Polymers (MIPs)

Molecularly Imprinted Polymers (MIPs) are polymers that have been modified in order to have a larger affinity for specific compounds. These MIPs can be applied as a coating to electrochemical sensors and as a result, the sensor has a higher specificity for the analytes of interest. Examples have shown to be successful for the detection of for example PFOS and microorganisms in water. A large challenge within the MIPs is the formation of homogeneous receptors with equal affinity on a large scale.